

Alexandar Pavlovic, BSc

# **Didactic thorax phantom for the simulation of ECG**

## **Master thesis**

for the award of the academic degree of  
Diplom-Ingenieur



## **Institute of Biomedical Imaging**

Stremayrgasse 16/III  
A-8010 Graz

Supervisor: Ao.Univ.-Prof. Dipl.-Ing. Dr. techn. Hermann Scharfetter

Reviewer: Ao.Univ.-Prof. Dipl.-Ing. Dr. techn. Hermann Scharfetter

Graz, November 2024

## **AFFIDAVIT**

I declare that I have authored this thesis independently, that I have not used other than the declared sources/resources, and that I have explicitly indicated all material which has been quoted either literally or by content from the sources used. The text document uploaded to TUGRAZonline is identical to the present master's thesis.

---

Date, Signature

## Abstract

Title: Didactical thorax phantom for simulating of ECG

For the laboratory exercise "Grundlage der Biomedizinischen Technik", a system is to be developed in which an ECG- signal is generated for a thorax phantom and this is to be produced using a PC. The microcontroller has the task of sending and receiving signals. With a voltage-controlled current source, the ECG signals can be transmitted to the thorax phantom. The Einthoven leads are measured on the phantom and passed to the microcontroller by using a circuit. This is then displayed in MATLAB. The hardware is installed in a suitable housing and is used for the laboratory exercise.

Keywords: ECG- Signal, voltage-controlled current source, MATLAB, Microcontroller, Einthoven leads, laboratory exercise

## Zusammenfassung

Titel: Didaktes Thoraxphantom zur Simulation von EKG

Für die Laborübung „Grundlage der Biomedizinischen Technik“ soll ein System entwickelt werden, mit dem EKG- Signale an einem physikalischen 3-D- Thoraxphantom generiert werden. Sowohl Signalgenerierung als auch -anzeige sollen mittels eines PC unter MATLAB erfolgen. Die Ansteuerung der Stromquellen und die Signalakquisition werden durch einen Microcontroller übernommen. Der Microcontroller hat die Aufgabe, Signale zu senden und zu empfangen. Mit einer spannungsgesteuerten Stromquelle können Quellströme in Form eines angenäherten Strom- Dipols (Herzvektor) in das Thoraxphantom eingespeist werden. Es werden die Einthoven- Ableitungen am Thoraxphantom mit einem Instrumentierungsverstärker gemessen und vom Microcontroller digitalisiert. Anschließend werden die Daten an den PC in das MATLAB-Frontend übertragen und dort dargestellt.

Schlüsselwörter: EKG- Signal, spannungsgesteuerten Stromquelle, MATLAB, Microcontroller, Einthoven- Ableitungen, Laborübung

## Acknowledgement

I would like to thank the following people who supported me in completing my Master's thesis:

Firstly, I would like to thank Ao.Univ.-Prof. Dipl.-Ing. Dr.techn. Hermann Scharfetter for his supervision, support and assessment. Thank you for the helpful and instructive discussions during the realisation of the Master's thesis.

I would also like to thank Walter Gmeindl, who always came up with good solutions to problems and was therefore able to implement them quickly. I would also like to thank the entire Biomedical Imaging Institute.

Thanks also to my friends who motivated and supported me throughout my studies.

Finally, I would like to thank my sisters who actively motivated me to stay on the ball and not despair. Special thanks go to my parents, who made my studies possible and supported me in every situation and encouraged me to keep going and not lose sight of my goal. Hvala vam puno za sve!!!

# Contents

1. Introduction.....	1
2. Methods.....	2
2.1. Generation of the source currents .....	2
2.2. MATLAB program.....	3
2.2.1. GUI .....	3
2.2.2. Measurement 1: Position type determination .....	6
2.2.3. Measurement 2: Cardiac vector reconstruction.....	8
2.2.4. Display button .....	8
2.2.5. Reset button.....	8
2.3. Microcontroller.....	9
2.3.1. DAC .....	10
2.3.2. ADC .....	12
2.3.3. USART .....	12
2.3.4. Program of the microcontroller .....	13
2.3.4.1. Receiving and converting data.....	13
2.3.4.2. Starting the DAC .....	13
2.3.4.3. Receiving analogue signals .....	14
2.3.4.4. Sending data.....	14
2.3.4.5. Signal inverting .....	15
2.3.4.6. Reset .....	15
2.4. Howland current source (voltage controlled current source) .....	16
2.5. Instrumentation amplifier .....	29
2.6. Supply .....	34
2.7. Electrodes .....	36
2.8. Determination of the conductivity of the NaCl solution .....	44
3. Results .....	46

3.1.	Howland current source .....	46
3.2.	Instrumentation amplifier .....	53
3.3.	Electrodes .....	56
3.4.	Measurement of the entire system .....	66
4.	Discussion .....	70
5.	Literature .....	72

## List of illustrations

Figure 1: schematic structure .....	2
Figure 2: GUI interface .....	3
Figure 3: Einthoven triangle- first derivation.....	5
Figure 4: Einthoven triangle - second derivation.....	5
Figure 5: Function call of the “Messung 1 starten” 1 button.....	7
Figure 6: Equation for converting the data.....	7
Figure 7: Technical features STM32F334C8 [26] .....	10
Figure 8: STM32F334 Nucleo-64 [8] .....	11
Figure 9: USART settings .....	12
Figure 10: Loop for data reception .....	13
Figure 11: Starting the DAC's .....	13
Figure 12: Starting the ADC.....	14
Figure 13: Basic Howland source .....	16
Figure 14: Basic Howland current source circuit.....	18
Figure 15: Improved Howland current source .....	19
Figure 16: Mirrored Enhanced Howland Currente Source (MEHCS) [3].....	21
Figure 17: improved Howland current source with 180° phase shift .....	22
Figure 18: Stability problems LM358 .....	23
Figure 19: open- loop simulation circuit with LM358 .....	24
Figure 20: Bode Plot of the non-mirrored Howland source with LM358.....	24
Figure 21: Bode Plot of the mirrored Howland source with LM358.....	25
Figure 22: open-loop simulation of the TL072 operational amplifier .....	26
Figure 23: Bode diagram of non- mirrored Howland source with TL072.....	26
Figure 24: Bode diagram of mirrored Howland source with TL072.....	27
Figure 25: Illustration of 1 dB compression point [13].....	27
Figure 26: Level converter circuit.....	28
Figure 27: Circuit diagram of the INA115 instrumentation amplifier.....	29
Figure 28: Driven Right Leg from the data sheet [16] .....	30
Figure 29: High pass filter .....	31
Figure 30: Low pass filter .....	32
Figure 31: Notch filter .....	33

Figure 32: Dual supply circuit with virtual ground [19] .....	34
Figure 33: Supply circuit with switching relay .....	35
Figure 34: Equivalent circuit diagram electrode-electrolyte junction [20] .....	36
Figure 35: Structure of a frequency response analyser [22 p.102] .....	37
Figure 36: Measurement setup for impedance spectroscopy and voltammetry [14].	38
Figure 37: Parameter settings for impedance spectroscopy .....	39
Figure 38: Cyclic voltammetry [24] .....	40
Figure 39: Voltammetry parameters set .....	41
Figure 40: Instrument for the conductivity of the electrolyte .....	45
Figure 41: Circuit diagram of the first Howland current source .....	47
Figure 42: Circuit diagram of the second Howland current source .....	48
Figure 43: Circuit diagram of the third Howland current source .....	49
Figure 44: Howland current source at a load of 2,2 k $\Omega$ .....	50
Figure 45: Measurement at 10 $\Omega$ and 11 V <sub>pp</sub> .....	51
Figure 46: Compression measurement at 1 Hz .....	52
Figure 47: Compression measurement at 10 Hz .....	52
Figure 48: Compression measurement at 20 Hz .....	52
Figure 49: Compression measurement at 50 Hz .....	52
Figure 50: Compression measurement at 100 Hz .....	52
Figure 51: Measurement of the Einthoven lead 3 with noise component .....	53
Figure 52: Measurement of the Einthoven lead 1 .....	54
Figure 53: Measurement of the Einthoven lead 2 .....	54
Figure 54: Measurement of the Einthoven lead 3 .....	55
Figure 55: Electrochemical impedance spectroscopy of an Ag/AgCl electrode .....	56
Figure 56: Voltammetry measurement of the brass sphere .....	57
Figure 57: Voltammetry measurement of the brass chrome-plated sphere .....	58
Figure 58: Voltammetry measurement of the stainless steel sphere .....	59
Figure 59: Voltammetry measurement of the stainless steel gold-plated sphere .....	60
Figure 60: Voltammetry measurement of the own silver-silver chloride sphere .....	61
Figure 61: New voltammetry programme settings .....	62
Figure 62: Voltammetry measurement of the own silver-silver chloride sphere with new settings .....	63
Figure 63: Voltammetry measurement of the disposable electrode silver-silver chloride electrodes .....	64



Figure 64: Cross with disposable electrodes .....	65
Figure 65: Einthoven leads of the patient patient245/s0480_re [27] .....	67
Figure 66: Measurement 1 with weighting $x = 1$ , $y = 1$ and $z = 1$ .....	67
Figure 67: Measurement 2.....	67
Figure 68: Axis type with weighting $x = 1$ , $y = 1$ and $z = 1$ .....	67
Figure 69: Axis type for measurement 2 .....	67
Figure 70: Measured vector loop measurement 2 .....	68
Figure 71: Original vector loop measurement 2.....	69

## List of tabels

Table 1: Measurement results of the first Howland current source .....	47
Table 2: Measurement results of the second Howland current source.....	48
Table 3: Measurement results of the third Howland current source .....	49

## List of abbreviations

ECG ... Electrocardiogram

kB ... kilobyte

ADC ... analogue-to-digital converter

DAC ... digital-to-analogue converter

MHz ... megahertz

GUI ... Graphic User Interface [1]

Guide ... graphic user interface design environment [2]

MECHS ... Mirrored Enhanced Howland Current Source [3]

NaCl ... sodium chloride

s ... Second

ms ... milliseconds

Hz ... Hertz

V ... Volt

mV ... millivolts

DRL ... Driven right leg

CMRR ... Common Mode Rejection Ratio (= DC voltage suppression)

DC offset ... DC voltage offset

MΩ ... Megaohm

nF ... Nanofarad

pF ... Pikofarad

kΩ ... Kiloohm

EIS ... Electrochemical Impedance Spectroscopy

USART ... universal synchronous and asynchronous serial receivers and transmitters  
[28]

mA ... milliamperes

dB ... Decibel

$\Omega$  ... Ohm

$\mu\text{F}$  ... microfarad

kHz ... kilohertz

V/s ... Volt per second

u ... atomic mass unit

mol ... unit of the amount of substance

$\text{cm}^2$  ... square centimetre

g ... gram

ml ... millilitre

$\text{cm}^3$  ... cubic metre

S ... Siemens

mS ... millisiemens

cm ... centimetres

$V_{pp}$  ... Volt peak peak

$\text{mV}_{pp}$  ... Millivolt peak peak

$\text{mA}_{pp}$  ... Milliampere peak peak

mA ... Milliampere

Ag/AgCl ... silver silver chloride

## 1. Introduction

The heart has an important function in the human body. It pumps blood through the body and supplies the organs with oxygen. A well-functioning heart is therefore of great importance. Unfortunately, heart disease is not uncommon. The electrocardiogram (ECG) is often used to recognise and treat diseases in good time. The ECG provides information on possible anatomical changes. Electrical currents are generated by excitation and regeneration of the heart and voltages can be measured on the body surface.

In the laboratory exercise "Fundamentals of Biomedical Engineering", the reconstruction of the vectorcardiogram and the standard derivation according to Einthoven with axis type determination are to be developed. In this work, the use of MATLAB (The MathWorks, Inc.) is specified. In the laboratory exercise, a thorax phantom filled with physiological saline solution is used. Three dipole electrodes are used as a substitute heart. The corresponding data is sent to the microcontroller via MATLAB. The microcontroller processes this data and the dipoles are controlled using voltage-controlled current sources. The leads can be measured on the surface of the thorax phantom and the measured voltages are amplified using instrumentation amplifiers. The amplified voltages are transferred to the microcontroller, processed and then the processed data is transferred to MATLAB and displayed.

The following tasks have to be carried out:

- Design a GUI in MATLAB
- Design a voltage controlled current source (Howland current source) with 10 mA<sub>pp</sub> and a frequency of 1 Hz.
- Source electrode area for generation of the source current
- Three ECG amplifiers for signal acquisition
- Microcontroller with three DAC, three ADC and GPIO's

## 2. Methods

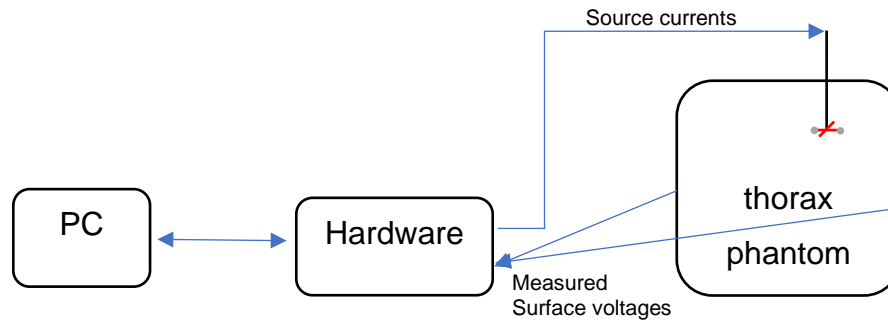


Figure 1: schematic structure

As per the task definition, the schematic structure is shown in figure 1.

### 2.1. Generation of the source currents

To take measurements on the surface of the thorax phantom, a source signal must be fed in. Therefore, ECG data is required. As mentioned in selection 1, the use of MATLAB (The MathWorks, Inc.) is specified in this thesis, therefore MATLAB data from the PhysioBank ATM database is used. The data set contains the derivatives according to Einthoven (I, II, III), Goldberger (aVL, aVR, aVF), Wilson (V1 - V6) and Frank (Vx, Vy, Vz). In both measurements, a signal period is cut out and repeatedly emitted until the digital-to-analogue converters (=DAC) is switched off.

Measurement 1 is used to determine and change the axis type. A source vector is fed in so that the Einthoven lead can be measured and by different weightings of the components different axis types are obtained. In the literature, there is no explicit data for a source vector, so the three Frank leads were used in a first approximation because they are a projection into the cartesian coordinate system and can be used as x-y-z components. Instead of an actual source signal, the Frank lead is taken as a substitution. This is not a real source vector but an approximation. The x-y-z components are associated with the x-y-z dipole signal. The purpose of the exercise

is to get a feel for what a layer type looks like and how the layer type changes with different weightings.

The main exercise is measurement 2. The source vector is not an arbitrary signal, but a clearly defined signal. The source vector is reconstructed from the measurement data of an ECG signal. When the reconstructed source vector is fed in, this ECG signal should be measured again under the assumption of an infinitely extended, homogeneously conductor around the source. The Einthoven derivation is used to reconstruct the source vector.

## 2.2. MATLAB program

### 2.2.1. GUI

The graphical user interface was created using the MATLAB tool guide.

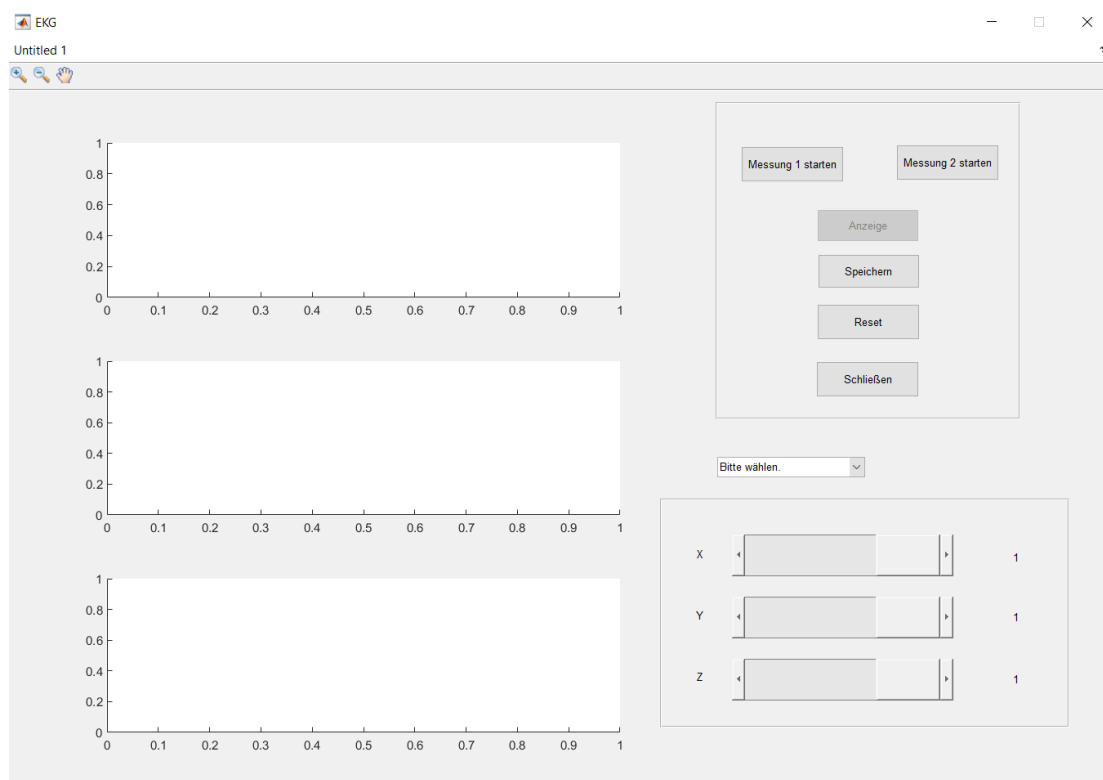


Figure 2: GUI interface

Figure 2 shows the structure of the graphical user interface. Here, the three measured signals are displayed in `plot_graph_1`, `plot_graph_2` and `plot_graph_3`. Whether measurement 1 or measurement 2 is to be carried out is selected in the pop-up menu. The buttons and the three slide bars are each positioned on a 'panel'. This has the advantage that you can move the respective buttons and slide bars as a unit during the development phase. In measurement 1, the slide bars are used so that each individual signal (x, y and z) can be multiplied by a value of '-1', '0' and '1', allowing the signals to be mirrored or the amplitudes to be reduced. The slide bars are deactivated for measurement 2. The first part of the laboratory exercise is started with the measurement 1 button and the second part of the laboratory exercise is started with the measurement 2 button. The Reset button is used to restore the initial state. The Save button is used to save the plots. The Close button can be used to close the GUI. The Display button is used to display the position type for measurement 1 and the position type and vector loop for measurement 2.

The source dipole is to be reconstructed from the data set, in this case the Einthoven leads of the patient data, for each point in time of the ECG. Since only two-dimensional measurement data is available, a two-dimensional reconstruction is also required. This means that the z component is redundant. The measurement vector  $\mathbf{v}$  represents the Einthoven derivatives (see eq. (1)) and the source vector  $\mathbf{q}$  corresponds to the x and y axes of the Cartesian coordinate system (see eq. (2)).

$$\mathbf{v} = \begin{bmatrix} E1 \\ E2 \end{bmatrix} \quad (1)$$

$$\mathbf{q} = \begin{bmatrix} x \\ y \end{bmatrix} \quad (2)$$

The measurement vector  $\mathbf{v}$  results from the multiplication of the construction matrix  $\mathbf{A}$  and the source vector  $\mathbf{q}$  (see eq. (3)).

$$\text{Measurement vector } \mathbf{v} = \text{Construction matrix } \mathbf{A} * \text{Source vector } \mathbf{q} \quad (3)$$



Since only measurement data or only one measurement vector  $v$  is available, the inverse of the construction matrix  $A$  must be formed and multiplied by the measurement vector to obtain the source vector (see eq. (4)). The inverse construction matrix is the reconstruction matrix.

$$q = A^{-1} * v \quad (4)$$

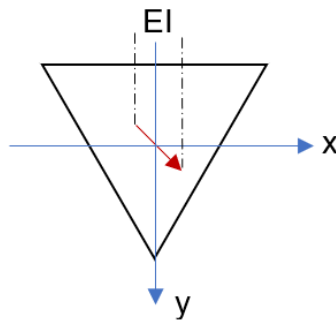


Figure 3: Einthoven triangle- first derivation

Firstly, an Einthoven triangle was drawn and an X-Y coordinate system was placed on it. A dipole vector was then drawn and a projection was made onto the Einthoven triangle. The first Einthoven derivative shows that the derivative only points in the x-direction (see figure 3).

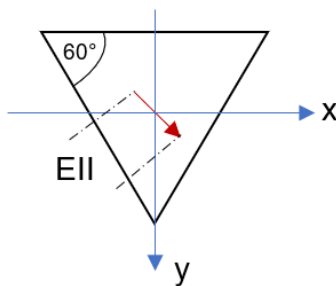


Figure 4: Einthoven triangle - second derivation

The second Einthoven derivative has both an x- and y- component (see figure 4). The x-axis is the adjacent leg of the triangle and the y-axis is the opposite leg if the second

derivative of the Einthoven triangle is the hypotenuse. This means that the x component is multiplied by the cosine of 60° (corresponds to 0.5) and the y component is multiplied by the sine of 60° (corresponds to root three half). This results in the following construction matrix.

The construction matrix A looks as follows:

$$A = \begin{bmatrix} 1 & 0 \\ 0,5 & \frac{\sqrt{3}}{2} \end{bmatrix} \quad (5)$$

The reconstruction matrix (inverse of the construction matrix) looks as follows:

$$A^{-1} = \begin{bmatrix} 1 & 0 \\ -\frac{1}{\sqrt{3}} & \frac{2}{\sqrt{3}} \end{bmatrix} \quad (6)$$

The source vector is calculated according to (7), (8) and (9):

$$\mathbf{q} = \begin{bmatrix} x \\ y \end{bmatrix} = \begin{bmatrix} 1 & 0 \\ -\frac{1}{\sqrt{3}} & \frac{2}{\sqrt{3}} \end{bmatrix} * \begin{bmatrix} E1 \\ E2 \end{bmatrix} \quad (7)$$

$$x = E1 \quad (8)$$

$$y = \left(-\frac{1}{\sqrt{3}}\right) * E1 + \frac{2}{\sqrt{3}} * E2 \quad (9)$$

### 2.2.2. Measurement 1: Position type determination

This subselection refers to [5].

Measurement 1 can be used to determine the position type of the heart. Depending on how the slide bars are set, the position type can be changed in the corresponding direction.

Firstly, measurement 1 must be selected from the pop-up menu. The respective buttons are activated and deactivated using a switch case statement. The slider bars are set to '1' at the start of measurement 1 and can take the values '0' and '-1'. The measurement is started by pressing the “Messung 1 starten” button. This calls up the 'data\_send' function (see figure 5).

```
[Vx_int, Vy_int, Vz_int] = data_send(inputdata, offset, x, y, z);
```

Figure 5: Function call of the “Messung 1 starten” 1 button

Firstly, a period of the ECG curve is determined and saved in variables. Then the absolute maximum and minimum values of the x, y and z data are determined in order to determine the range of the maximum amplitude of the signals. This is necessary to maintain the proportions of the signals.

```
Vx_data = int16((Vx - mean(Vx)) / range * 2048 + 2047);
Vy_data = int16((Vy - mean(Vy)) / range * 2048 + 2047);
Vz_data = int16((Vz - mean(Vz)) / range * 2048 + 2047);
```

Figure 6: Equation for converting the data

As can be seen in figure 6, the individual data sets are adjusted using the mean value, as the mean value was assumed to be the virtual zero point of the respective data set. Furthermore, the data is normalised and converted into an Int16 number. The conversion is necessary to be able to map the data in a value range from -1 to 1 to an integer range from 0 to 4095. This is necessary to send the data to a 12 bit DAC with unipolar output. It is also necessary to raise the zero line to the value 2047 in order to be able to display negative values.

The values of the individual signals are then converted into a string and separated by commas. As the microcontroller only has 64 kB of memory available, every third value was taken in the individual data records, thus solving the problem of the microcontroller's memory being too small. To send the data, the three individual strings are written in one large string, where they are separated by semicolons. An 'x' is added as the last symbol, symbolising the end of the string. The serial communication port is then opened and the data is sent to the microcontroller. The programme then waits in a while loop until the results of the measurement are received from the microcontroller. In this while loop, each individual symbol of the received data set is run through. The values of the data set are again separated by commas and semicolons. The x, y and z values of the data set are split by if and else conditions and converted into the data type double. When the 'x' symbol has been read, the while loop is interrupted, the port

is closed and the function is terminated. The function returns the measured values and these are displayed on the GUI.

### 2.2.3. Measurement 2: Cardiac vector reconstruction

The source vector calculation is described in section 2.2.1. The slide bars are deactivated for measurement 2, as no weighting is required. Data processing, as well as sending and receiving data, follows the same principle as in subsection 2.2.2. The function returns the measured values and these are displayed on the GUI.

### 2.2.4. Display button

The display button shows the location type for measurement 1 and the axis type and the measured and original vector loops for measurement 2. For both measurements, the position type is displayed in a separate plot window and for measurement 2, the vector loop of the measured values and the original values are also displayed in separate plot windows.

### 2.2.5. Reset button

The reset button is used to reset the GUI and should be pressed after each measurement.

### 2.3. Microcontroller

The requirement for this work is to work with a microcontroller of the type STM32. For the application on the Thoraxphantom, it is important that a signal is sent in all three levels, so a microcontroller with three digital-to-analogue converters (= DAC) must be used. The STM homepage was used to search for a suitable microcontroller. There were two Nucleo boards to choose from, namely the STM32F334 and the STM32G474. The main difference between the two boards is the flash memory and the SRAM memory. The STM32F334 has a flash memory of 64 kB and an SRAM memory of 12 kB. In contrast, the STM32G474 has a flash memory of 512 kB and an SRAM memory of 96 kB [6]. Due to the long ordering time of the STM32G474, the STM32F334 board was chosen.

Figure 7 provides an overview of the technical features of the STM32F334C8.

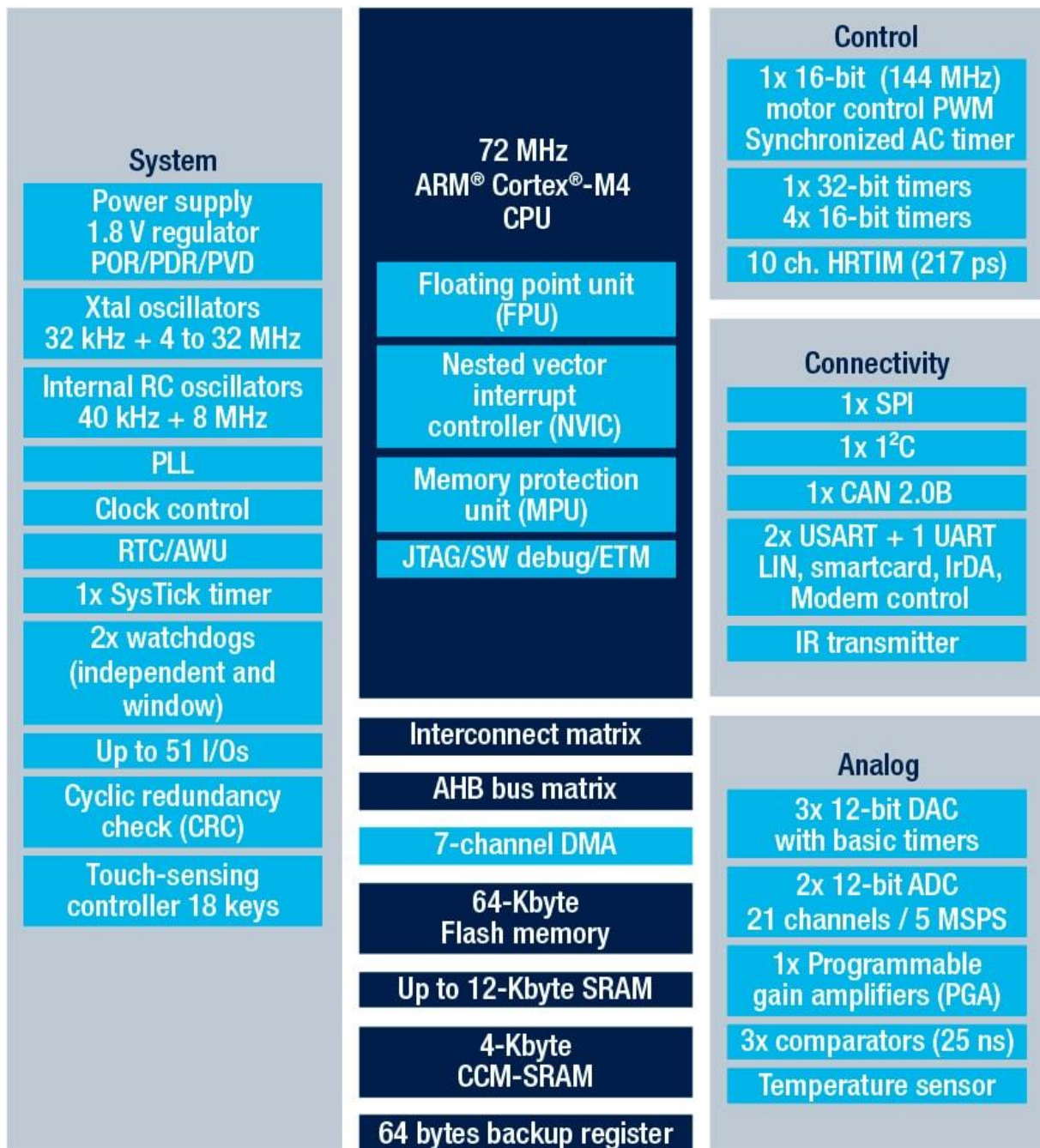


Figure 7: Technical features STM32F334C8 [26]

### 2.3.1. DAC

The DACs are used to convert the processed digital values into analogue signals. As the human heart beats approximately 60 times per minute at rest, the DAC timers must be set so that the analogue signal has a period of 1 s. According to the data sheet, the Nucleo board has three 12-bit DAC. The timers of the three DACs (DAC 1 Channel 1,

DAC 1 Channel 2 and DAC 2 Channel 1) are controlled by APB1 timer clock. DAC 1 Channel 1 is triggered via timer 6, DAC 1 Channel 2 via timer 3 and DAC 2 Channel 1 via timer 7. The APB1 timer clock is set to 30 MHz. The prescalers of timer 3, timer 6 and timer 7 are set to 300 and the counter period is set to 280. 355 values are output per channel and the period duration of the timers is calculated in equation (10) as follows.

$$T = \frac{APB\ 1\ timer\ clock}{Prescaler * Counter\ Period * n} = \frac{30\ MHz}{300 * 280 * 355} = 1\ s \quad (10)$$

n ... number of samples

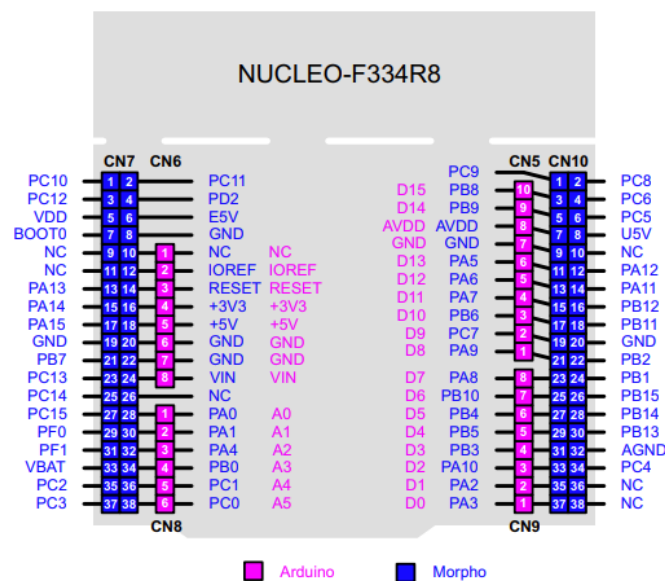


Figure 8: STM32F334 Nucleo-64 [8]

The DAC outputs A2, D13 and D12 are on the Nucleo board (see figure 8). This converts the transferred MATLAB data into an analogue signal and outputs it with a period of one second. The DAC outputs are connected to the Howland sources.

### 2.3.2. ADC

An ADC is required to digitize the measured analogue signals from the thorax phantom on the computer. According to the data sheet, the Nucleo board has two 12-bit ADCs with 21 channels [7]. Three ADC channels are required for the laboratory exercise, which can be realised with the STM32 without any problems. The ADC is triggered by timer 2. Two periods of the received signal are displayed. The timer settings are therefore the same as the DAC's timer settings, except that the counter period has been increased to 560 (see eq. (11)). This means that the period duration of the timer has been set to 0.5 s.

$$T = \frac{APB\ 1\ timer\ clock}{Prescaler * Counter\ Period * n} = \frac{30\ MHz}{300 * 560 * 355} = 0,5\ s \quad (11)$$

The ADCs are located on the Nucleo board A0, A1 and A5 (see selection 2.3.1. figure 8) and these ADC outputs are connected to the receiver unit on the board.

### 2.3.3. USART

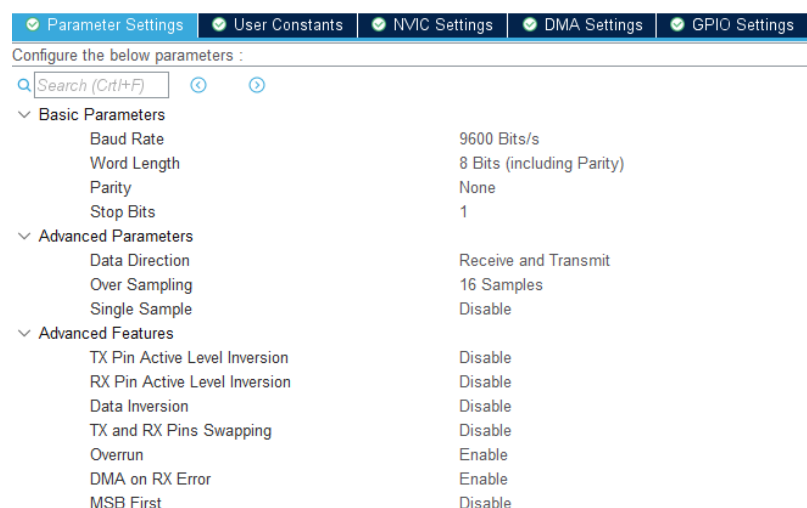


Figure 9: USART settings



USART is used for serial communication between the computer and microcontroller. Figure 9 shows the USART configuration. Each character consists of a start bit, 8 data bits and a stop bit, without a parity bit. This means that each character consists of 10 bits and with a baud rate of 9600 bits/s, 960 bytes/s can be transmitted, which is sufficient for the application.

#### 2.3.4. Program of the microcontroller

##### 2.3.4.1. Receiving and converting data

```

182   while (rx_finished)
183   {
184       HAL_UART_Receive_IT(&huart2, &rx_data, 1);
185
186       if (rx_finished == 0)
187       {
188           break;
189       }
190   }

```

Figure 10: Loop for data reception

As can be seen in figure 10, the function 'HAL\_UART\_Receive\_IT(&huart2, &rx\_data, 1);' is called in a while loop. In this function, the received symbols are checked and split into x-values, y-values and z-values. Next, the char arrays are converted into an integer array. When the final symbol 'x' is received, the while loop is interrupted.

##### 2.3.4.2. Starting the DAC

```

194   HAL_TIM_Base_Start(&htim6);
195   HAL_DAC_Start_DMA(&hdac1, DAC1_CHANNEL_1, Vx_int, counter_x, DAC_ALIGN_12B_R);
196   HAL_TIM_Base_Start(&htim3);
197   HAL_DAC_Start_DMA(&hdac1, DAC1_CHANNEL_2, Vy_int, counter_y, DAC_ALIGN_12B_R);
198   HAL_TIM_Base_Start(&htim7);
199   HAL_DAC_Start_DMA(&hdac2, DAC2_CHANNEL_1, Vz_int, counter_z, DAC_ALIGN_12B_R);
200

```

Figure 11: Starting the DAC's

Figure 11 shows that the respective timers are started with the corresponding DAC. Here, the x, y and z signals are output at the respective outputs of the microcontroller.

#### 2.3.4.3. Receiving analogue signals

```

203 HAL_TIM_Base_Start(&htim2); // timer für adc
204
205 while (adc_finished)
206 {
207     HAL_ADC_Start_DMA(&hadc1, get_buffer, 3);
208
209     if (adc_finished == 0)
210     {
211         HAL_ADC_Stop_DMA(&hadc1);
212         break;
213     }
214 }
215

```

Figure 12: Starting the ADC

In the next step, the timer of the ADC (timer 2) and the ADC are started (see figure 12). If a voltage is now present at the respective ADC inputs, the function `HAL_ADC_ConvCpltCallback(ADC_HandleTypeDef* hadc)` is called. In the function, each ADC channel is scanned individually and the measured signals are saved in the corresponding variables. When the last value is saved, the variable `adc_finished` is set to zero. This stops the ADC and cancels the while loop.

#### 2.3.4.4. Sending data

After the recorded data from the ADC has been saved, the data is sent to the computer. Using the `sprintf` command, the data is written to a char array and this array sends each individual symbol to MATLAB. An addition had to be added to the `sprintf` command, namely `"%04i"`. With this addition, numbers that do not have four digits are prefixed with as many zeros as necessary to create a four-digit number. An 'x' is appended to the last symbol to be transferred. This tells the MATLAB programme that the transfer can be completed.

#### 2.3.4.5. Signal inverting

Signal inverting is used to restore the silver-chloride layer of the electrodes. The purpose of signal inversion is to achieve an average value of zero. The idea will be described in selection 3.3 p. 65. In the first step, the timers of the DACs are stopped and reset. The individual signals are then mirrored, timers are started and the signals are output. The DACs are stopped after 15 seconds.

#### 2.3.4.6. Reset

After the signal mirroring is completed, the microcontroller is reset with the command `NVIC_SystemReset()`.

## 2.4. Howland current source (voltage controlled current source)

Selection 2.4. refers to [3,5,9,11,12,13].

The requirement for this work was to use a voltage-controlled current source. In [5] it was mentioned that the various signals interfered with each other when fed into the thorax phantom and it was suggested that the Howland current source could provide a remedy [5]. This would prevent any interference currents from influencing the signals [5]. The idea is that two Howland current source are operated push- pull mode. An electrode and a counter electrode are required for the x, y and z axes. This means that the current is emitted by the electrode and received by the counter electrode. This means that the signal from the counter electrode requires a phase shift of  $180^\circ$ .

The "Basic Howland" circuit was invented by Prof Bradford Howland at MIT around 1962 [9]. The function of the circuit is given if the feedback and positive feedback are equally strong, i.e. the resistance ratios  $R_2/R_1$  and  $R_4/R_3$  (see derivation) are equal [9].

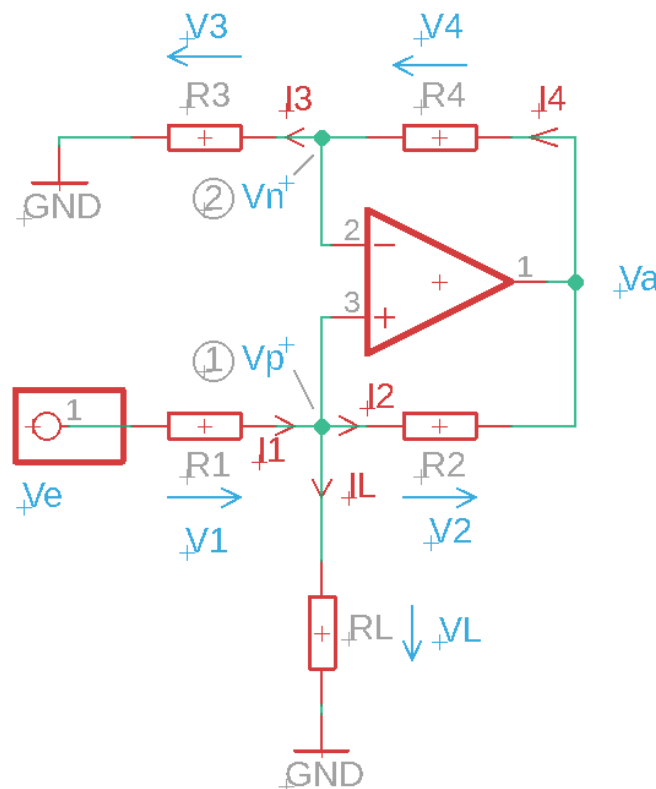


Figure 13: Basic Howland source

Derivation:

$$V_p = V_n = V \quad (12)$$

$$\textcircled{1}: I_1 = I_2 + I_L \quad (13)$$

$$I_L = I_1 - I_2 \quad (14)$$

$$I_L = \frac{V_e - V_p}{R_1} - \frac{V_p - V_a}{R_2} = \frac{V_e - V}{R_1} - \frac{V - V_a}{R_2} \quad (15)$$

$$\textcircled{2}: I_3 = I_4 \quad (16)$$

$$\frac{V_n}{R_3} = \frac{V}{R_3} = \frac{V_a - V_n}{R_4} = \frac{V_a}{R_4} - \frac{V_n}{R_4} = \frac{V_a}{R_4} - \frac{V}{R_4} \quad (17)$$

$$\frac{V_a}{R_4} = \frac{V}{R_3} + \frac{V}{R_4} \quad (18)$$

$$V_a = V * R_4 * \left( \frac{1}{R_3} + \frac{1}{R_4} \right) \quad (19)$$

$$V_a = V * \left( 1 + \frac{R_4}{R_3} \right) \quad (20)$$

$V_a$  in equation (15):

$$\textcircled{1}: I_L = \frac{V_e - V}{R_1} - \frac{V - V * \left( 1 + \frac{R_4}{R_3} \right)}{R_2} \quad (21)$$

$$I_L = \frac{V_e}{R_1} - \frac{V}{R_1} - \frac{V}{R_2} + \frac{V}{R_2} + \frac{V * R_4}{R_2 * R_3} \quad (22)$$

$$I_L = \frac{V_e}{R_1} - V * \underbrace{\left( \frac{1}{R_1} - \frac{R_4}{R_2 * R_3} \right)}_{\stackrel{!}{=} 0} \quad (23)$$

$$\frac{1}{R_1} - \frac{R_4}{R_2 * R_3} \stackrel{!}{=} 0 \quad (24)$$

$$\frac{1}{R_1} - \frac{R_4}{R_2 * R_3} = 0 \quad (25)$$

$$\frac{1}{R_1} = \frac{R_4}{R_2 * R_3} \quad (26)$$

$$\frac{R_2}{R_1} = \frac{R_4}{R_3} \quad (27)$$

If the resistance ratio is the same, then the following equation results:

$$I_L = \frac{V_e}{R_1} \quad (28)$$

The following paragraph refers to the quote [9].

The load current  $I_L$  depends on the input voltage  $V_e$  and the resistance  $R_1$ . Thus, the Howland source supplies a constant current, independent of the load, provided that the OPV does not saturate. The disadvantage of the circuit is that very precise resistors are required (0.1% or even 0.01%). Another disadvantage of the basic Howland source is the dynamic output range, namely if the load node  $V_p$  increases sharply, then the output of the operational amplifier must increase by twice as much. The result would be that the operational amplifier would saturate already at moderate signal levels. This disadvantage can be avoided by the "improved Howland source" circuit.

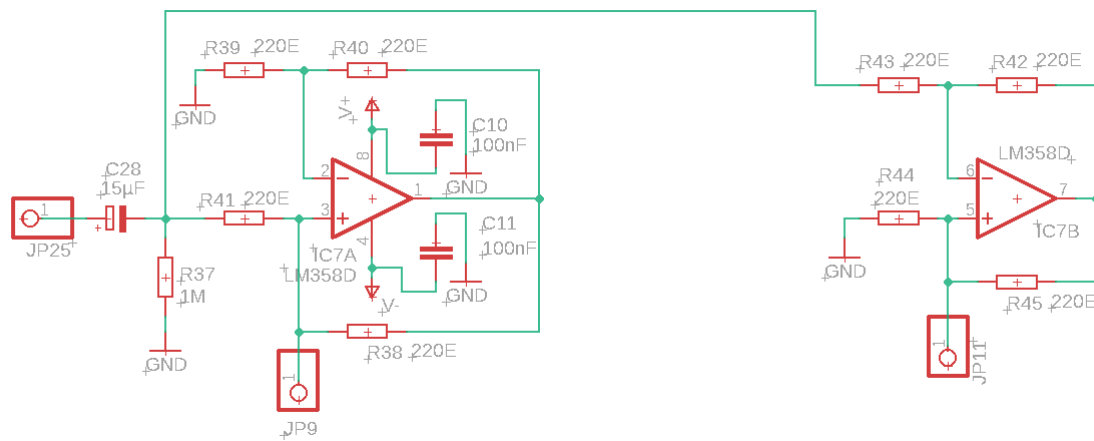


Figure 14: Basic Howland current source circuit

The circuit in figure 14 was set up and tested. Unfortunately, this design did not deliver the desired result, as the signal was not true to shape and there was no phase shift of  $180^\circ$  degrees between the source and sink. An alternative was therefore sought.

Next, the "improved Howland current source" was analysed. Figure 15 shows the "improved Howland current source".

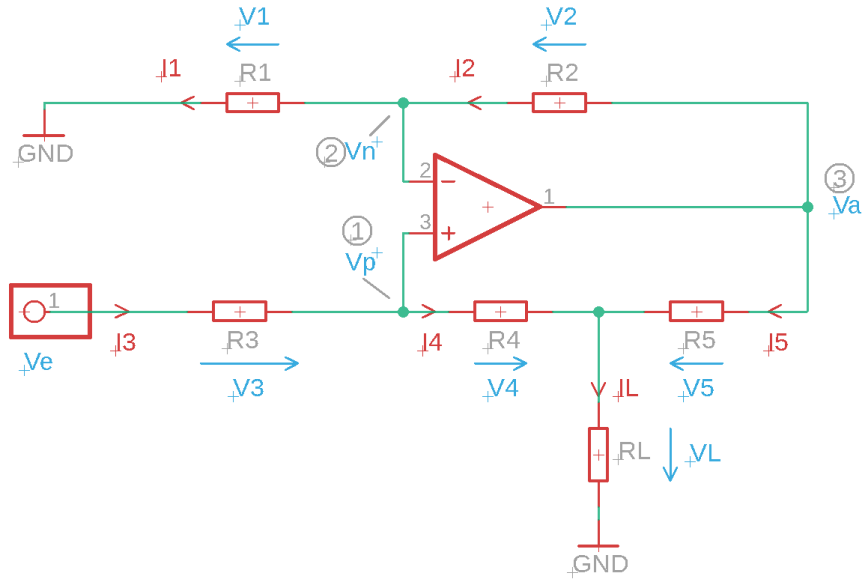


Figure 15: Improved Howland current source

Derivation:

$$\textcircled{1}: I_1 = I_2 \quad (29)$$

$$\frac{V_n}{R_1} = \frac{V_a - V_n}{R_2} \quad (30)$$

$$V_p = V_n = V \quad (31)$$

$$\frac{V_a}{R_2} = V * \left( \frac{1}{R_1} + \frac{1}{R_2} \right) \quad (32)$$

$$V_a = V * \left( 1 + \frac{R_2}{R_1} \right) \quad (33)$$

$$\textcircled{2}: I_3 = I_4 \quad (34)$$

$$\frac{V_e - V_p}{R_3} = \frac{V_p - V_L}{R_4} \quad (35)$$

$$\frac{V_e}{R_3} - \frac{V}{R_3} = \frac{V}{R_4} - \frac{V_L}{R_4} \quad (36)$$

$$\frac{V_L}{R_4} = V * \left( \frac{1}{R_3} + \frac{1}{R_4} \right) - \frac{V_e}{R_3} \quad (37)$$

$$V_L = V * \left( 1 + \frac{R_4}{R_3} \right) - V_e * \frac{R_4}{R_3} \quad (38)$$

$$\textcircled{3}: I_L = I_4 + I_5 \quad (39)$$

$$I_L = \frac{V_p - V_L}{R_4} + \frac{V_a - V_L}{R_5} \quad (40)$$

$$I_L = \frac{V}{R_4} - \frac{V_L}{R_4} + \frac{V_a}{R_5} - \frac{V_L}{R_5} \quad (41)$$

$V_L$  from equation (38) and  $V_a$  from equation (33) are used:

$$I_L = \frac{V}{R_4} - \frac{V * \left(1 + \frac{R_4}{R_3}\right) - V_e * \frac{R_4}{R_3}}{R_4} + \frac{V * \left(1 + \frac{R_2}{R_1}\right)}{R_5} - \frac{V * \left(1 + \frac{R_4}{R_3}\right) - V_e * \frac{R_4}{R_3}}{R_5} \quad (42)$$

$$I_L = \cancel{\frac{V}{R_4}} - \cancel{\frac{V}{R_4}} - \frac{V}{R_3} + \frac{V_e}{R_3} + \cancel{\frac{V}{R_5}} + \frac{V * R_2}{R_1 * R_5} - \cancel{\frac{V}{R_5}} - \frac{V * R_4}{R_3 * R_5} + \frac{V_e * R_4}{R_3 * R_5} \quad (43)$$

$$I_L = -\frac{V}{R_3} + \frac{V_e}{R_3} + \frac{V * R_2}{R_1 * R_5} - \frac{V * R_4}{R_3 * R_5} + \frac{V_e * R_4}{R_3 * R_5} \quad (44)$$

$$I_L = V_e * \underbrace{\left(\frac{1}{R_3} + \frac{R_4}{R_3 * R_5}\right)}_{\frac{R_4 + R_5}{R_3 * R_5}} + V * \underbrace{\left(-\frac{1}{R_3} + \frac{R_2}{R_1 * R_5} - \frac{R_4}{R_3 * R_5}\right)}_{\stackrel{!}{=} 0} \quad (45)$$

$$-\frac{1}{R_3} + \frac{R_2}{R_1 * R_5} - \frac{R_4}{R_3 * R_5} = 0 \quad (46)$$

Reduce  $R_5$  in denominator:  $\frac{R_2}{R_1 * R_5} = \frac{1}{R_3} + \frac{R_4}{R_3 * R_5} = \frac{R_4 + R_5}{R_3 * R_5}$  (47)

Resistance ratio:

$$\frac{R_2}{R_1} = \frac{R_4 + R_5}{R_3} \quad (48)$$

Resistance ratio Transform and insert into equation (45):

$$R_4 = \frac{R_2 * R_3}{R_1} - R_5 \quad (49)$$

$$I_L = V_e * \frac{\frac{R_2 * R_3}{R_1} - R_5 + R_5}{R_3 * R_5} = V_e * \frac{R_2 * R_3}{R_1 * R_3 * R_5} = V_e * \frac{R_2}{R_1 * R_5} \quad (50)$$

If  $R_1 = R_2$ , then the equation reads:

$$I_L = \frac{V_e}{R_5} \quad (51)$$

The following paragraph refers to [9].

With the "improved Howland source", the amplification and the output current are defined by the resistor  $R_5$  (see figure 15). The gain can be influenced by the ratio  $R_2/R_1$  (normally chosen as 1). This means that a smaller resistor value can be used for  $R_5$  and all other resistors can be high-impedance, which results in better CMRR behaviour. With the "improved Howland source", the ratio  $(R_4 + R_5) / R_3$  must be equal



to  $R_2 / R_1$ . To achieve this ratio,  $R_3$  or  $R_2$  can be increased by the value of  $R_5$ . Another possibility is to connect a potentiometer in series with  $R_3$  or  $R_2$ . In this case, a fixed solution was chosen, namely a resistor was connected in series to  $R_2$ , which corresponds to the value of  $R_5$ .

The circuit was built and tested on a breadboard. The circuit was more stable and the shape was also correct. The Mirrored Enhanced Howland Current Source (MEHCS) (see figure 16) was then tested.

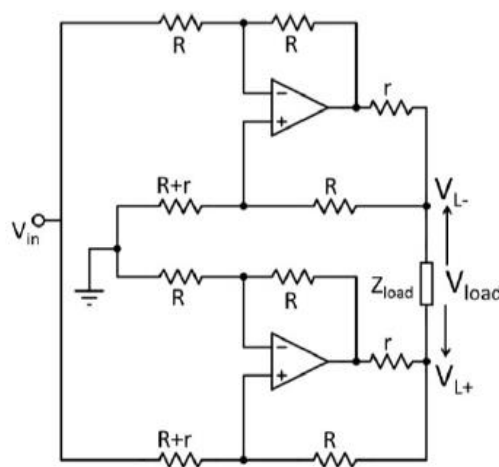


Figure 16: Mirrored Enhanced Howland Current Source (MEHCS) [3]

The circuit consists of two "improved Howland sources", which are connected in opposite polarity. The problem with the MEHCS version was that there was no phase shift of  $180^\circ$  between the source and sink.

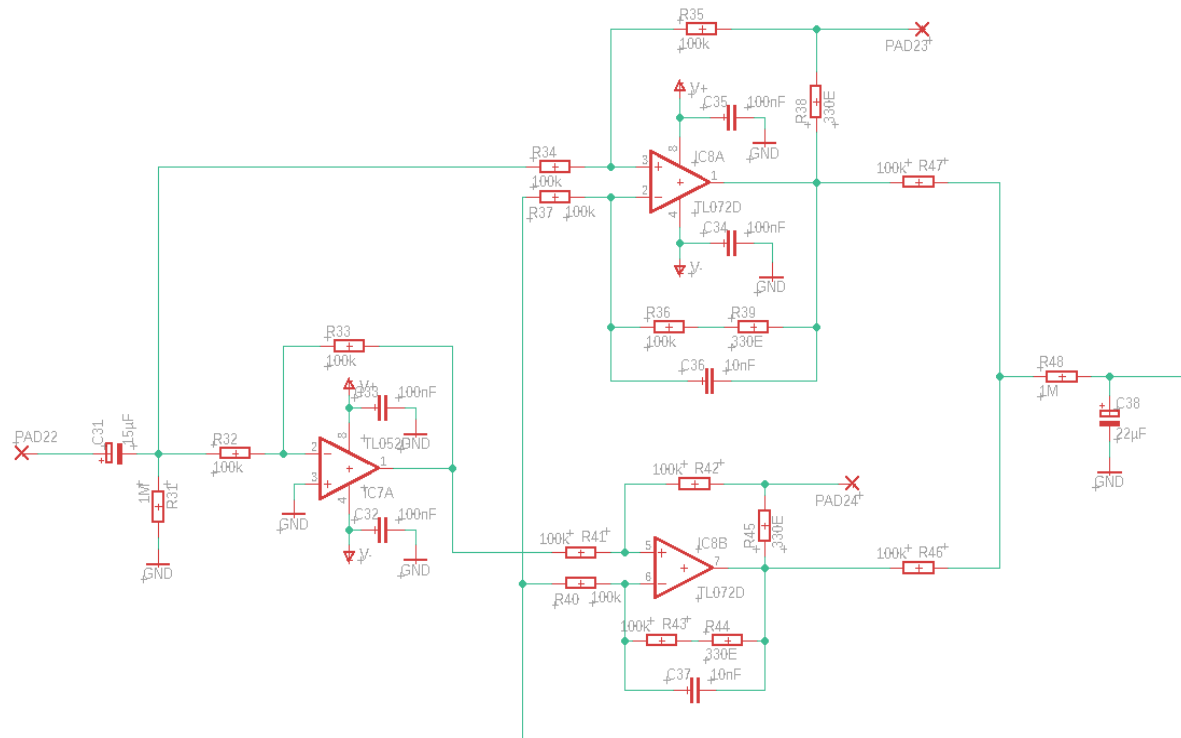


Figure 17: improved Howland current source with 180° phase shift

Next, the circuit in figure 17 was built and tested. The circuit consists of two improved Howland sources and an inverting amplifier and the load is connected between pad 23 and pad 24. The inverting amplifier is used to rotate the input signal by 180° and the phase-shifted signal is passed on to one of the two Howland sources. This results in two voltage-controlled current sources and a phase shift of 180°. The two capacitors in the feedback path of the Howland sources are used to smooth the signal and suppress noise. The cut-off frequency of the RC element is 159.2 Hz, allowing utilisation up to the cut-off frequency. In the classic version of the improved Howland source, the resistors of the inverting inputs of the operational amplifier are connected to ground. This leads to a DC voltage offset.

The following paragraph refers to [11].

Through an offset correction at the negative feedback, the operational amplifiers should provide an output voltage that is lower by this value and thus compensate for this DC voltage offset. This was realised by averaging a voltage divider. The voltage divider consists of two 100 kΩ resistors, so that the same voltage should drop across

both resistors. A low-pass filter is then connected, which has the task of filtering the alternating component in the case of alternating voltage signals.

According to the data sheet, the LM358 operational amplifier can provide a current of 40 mA as a source and sink [12]. The calculation of the output current is the same as for the "improved Howland source" (eq. (51)). The DAC of the STM32 can output a voltage of 3.3 V and the Howland source should deliver a current of 10 mA. The circuit was set to a current of 10 mA (see eq. (52)).

$$I_L = \frac{3,3 \text{ V}}{330 \Omega} = 10 \text{ mA} \quad (52)$$

The above-mentioned design has delivered the desired result of a phase shift of 180° between source and sink. Oscillations have occurred, especially at low loads, so the circuit has a stability problem (see figure 18).



Figure 18: Stability problems LM358

The LTSpice programme (Analog Devices, Inc) was used for the simulation. The open-loop amplification of the circuit was simulated for stability. Figure 19 shows the simulation model. The measuring points are o1, o2 (labelled yellow) and i1 (labelled green) is fed in.

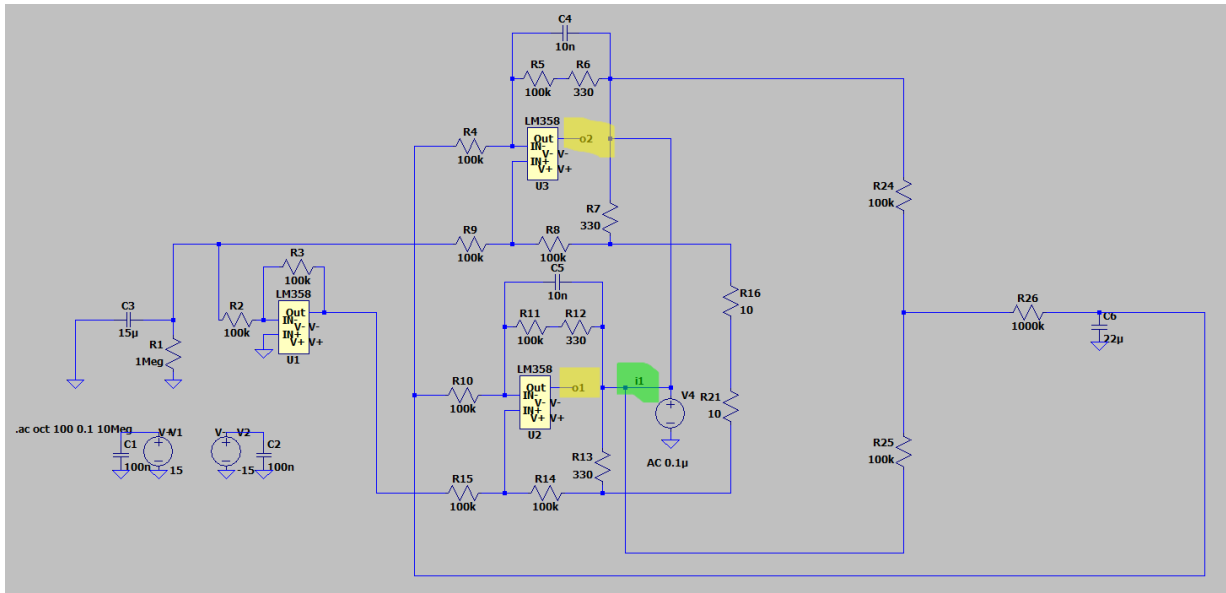


Figure 19: open- loop simulation circuit with LM358

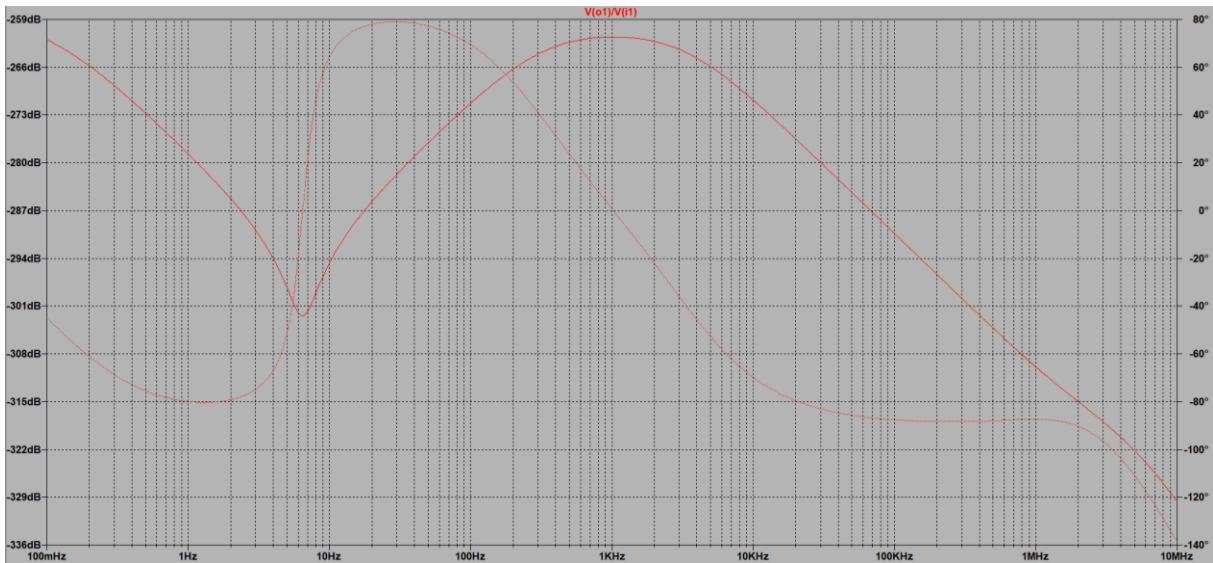


Figure 20: Bode Plot of the non-mirrored Howland source with LM358

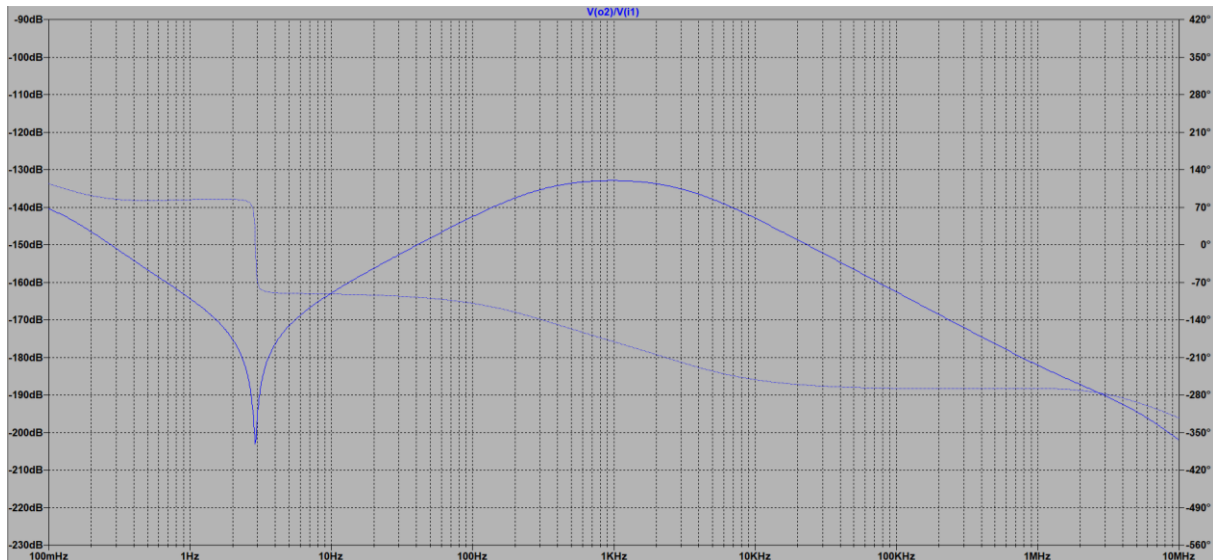


Figure 21: Bode Plot of the mirrored Howland source with LM358

The model of the LM358 was imported into LTSpice and the model is not working (see figure 20 and 21). The simulation does not provide a clear message because an open loop gain of -260 dB is not possible. According to the data sheet, the open loop gain should be 100 dB [12]. The cause could not be determined, but it is suspected that the model does not work in the complex circuit. For this reason, the simulation could not clarify where the stability problem lies. Since it did not work in practice, it was decided to use a different, more stable operational amplifier.

The next step was to look for another operational amplifier with the same pin assignment as the LM358.

A stability analysis was carried out on the following operational amplifiers:

- LMC6462
- MC1458
- OPA1013
- OPA2237
- TL052
- TL072
- TL082

Due to supply bottlenecks, the following operational amplifiers MC1458, OPA1013, TLC272, TL082 (wired) and TL072 were ordered and tested. Figure 22 shows the measuring points o1, o2 (labelled yellow) and i1 (labelled green).

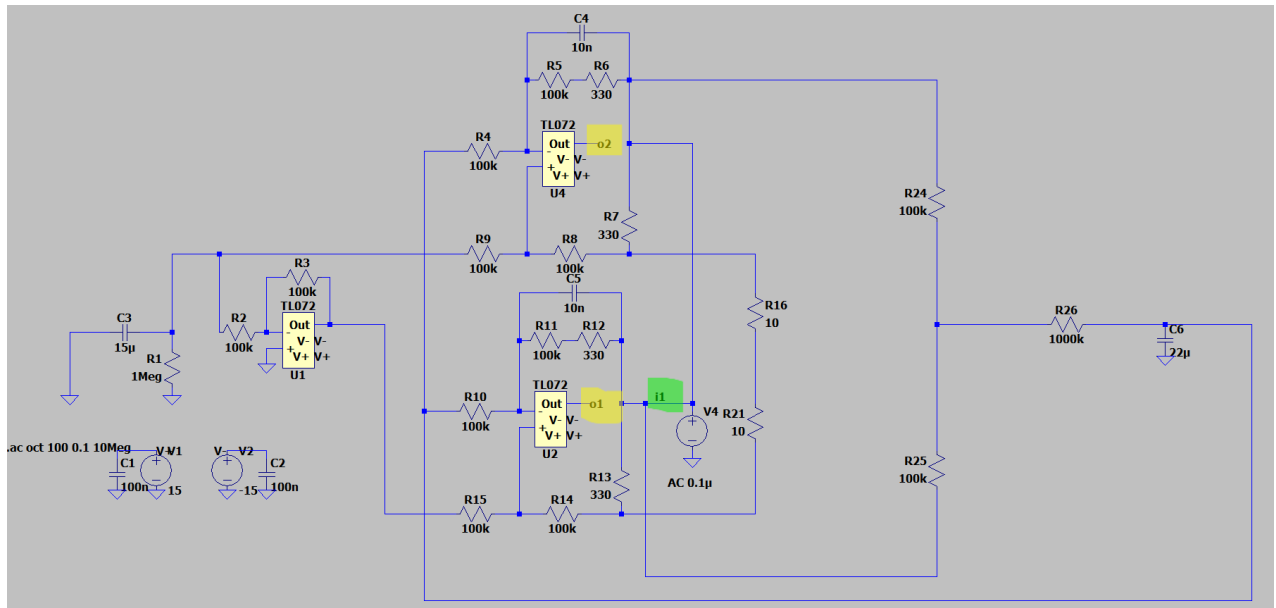


Figure 22: open-loop simulation of the TL072 operational amplifier

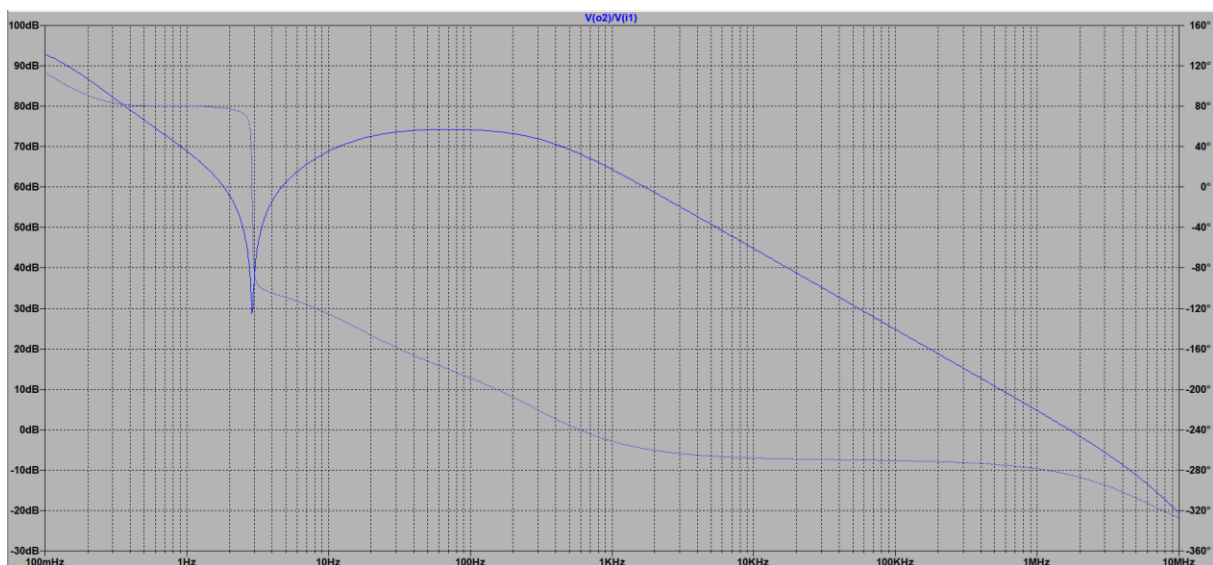


Figure 23: Bode diagram of non- mirrored Howland source with TL072

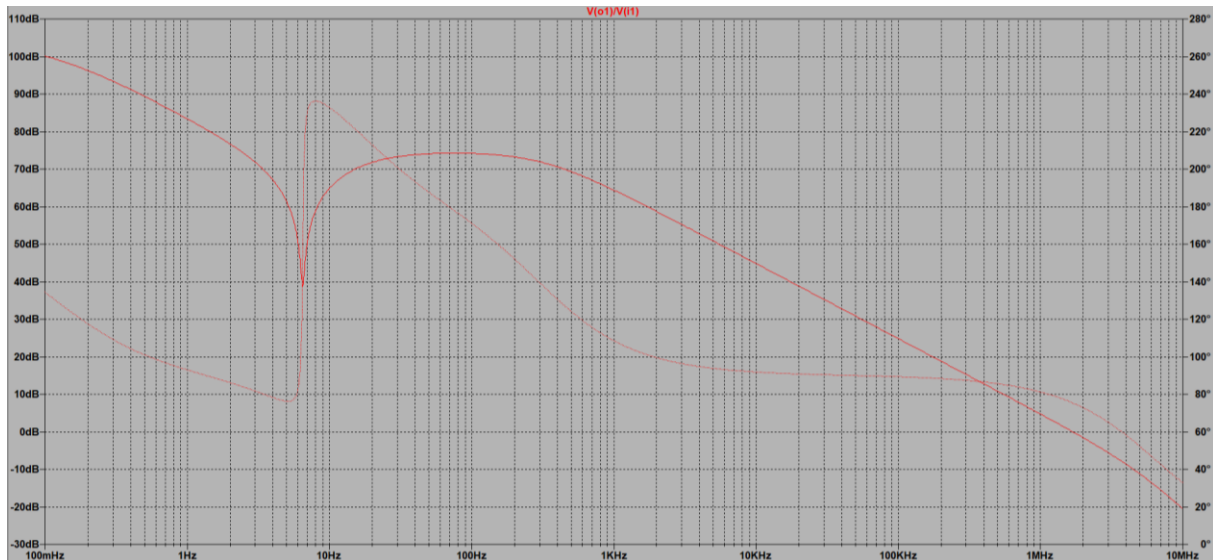


Figure 24: Bode diagram of mirrored Howland source with TL072

As can be seen in figures 23 and 24 above, the operational amplifier has an open loop gain of 100 dB at the start of the measurement. The decisive factor is the phase reserve of the operational amplifier at 0 dB. The TL072 has a phase reserve of around 75° at 0 dB. The TL072 operational amplifier has achieved the desired stability and a 180° phase shift between two Howland sources.

The compression point of the Howland sources was also determined. The compression point is determined when the real output power differs from the ideal output power of the amplifier by 1 dB [13]. To determine the compression point of the Howland source, a resistance of 18  $\Omega$  is applied to the source and the input voltage is varied from 0 to 11 V<sub>pp</sub> (in steps of 0.5 V<sub>pp</sub>). The current is measured with a digital multimeter and calculated. Figure 25 shows the graphical representation of the compression point.

Figure 25 redrawn and modified from [13].

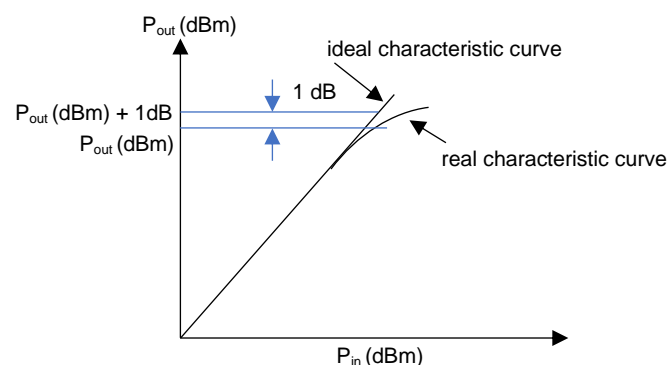


Figure 25: Illustration of 1 dB compression point [13]

Despite the use of a high-pass filter at the input of the Howland source, a small DC voltage offset occurs. As a DC voltage is permanently applied to the self-chlorinated spheres when they are switched on, this leads to degradation of the chloride layer. For this reason, the high-pass filter was replaced by a level converter so that the DC voltage can be adjusted more precisely. Figure 26 shows the structure of the level converter.

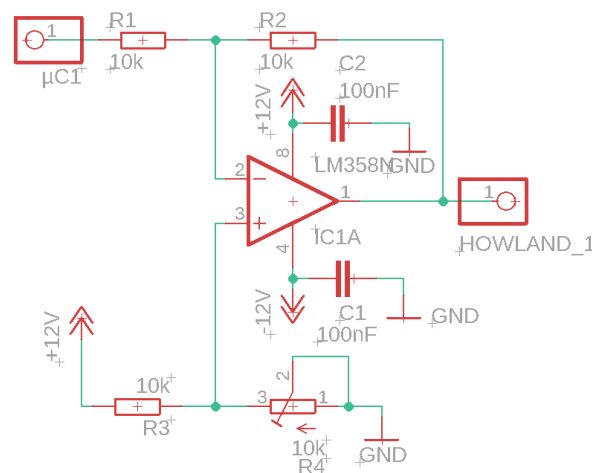


Figure 26: Level converter circuit

The gain of the level converter is -1. The input voltage of the Howland source can be raised or lowered using the potentiometer and thus the DC voltage component at the output of the Howland source can be reduced to zero.

The solution with the level converter has a single disadvantage. Since the DAC cannot represent negative voltages, the zero line is raised to the half output range of the DAC. The level converter brings the voltage back to the zero line. When the DAC has finished outputting the signal and is switched off (0 V), a DC voltage of the half output range is applied to the electrodes and causes electrolysis. As a result, the chlorine layer of one electrode decreases and at the other electrode in the same axes increases due to electrolyses. Selection 2.6. explains how this problem was solved.

The measurement results of the Howland current sources can be seen in selection 3.2.



## 2.5. Instrumentation amplifier

A crucial part of the ECG is the pre-amplification of a signal. On the one hand, the measurement voltage should be amplified to a usable range, which also amplifies the noise. On the other hand, a large part of the signal interference should be reduced or removed by correctly dimensioning the amplifier, resulting in a high common mode rejection ratio. An ECG signal is measured as the differential voltage of two electrodes, which is why an instrumentation amplifier or differential amplifier is required (see Figure 27).

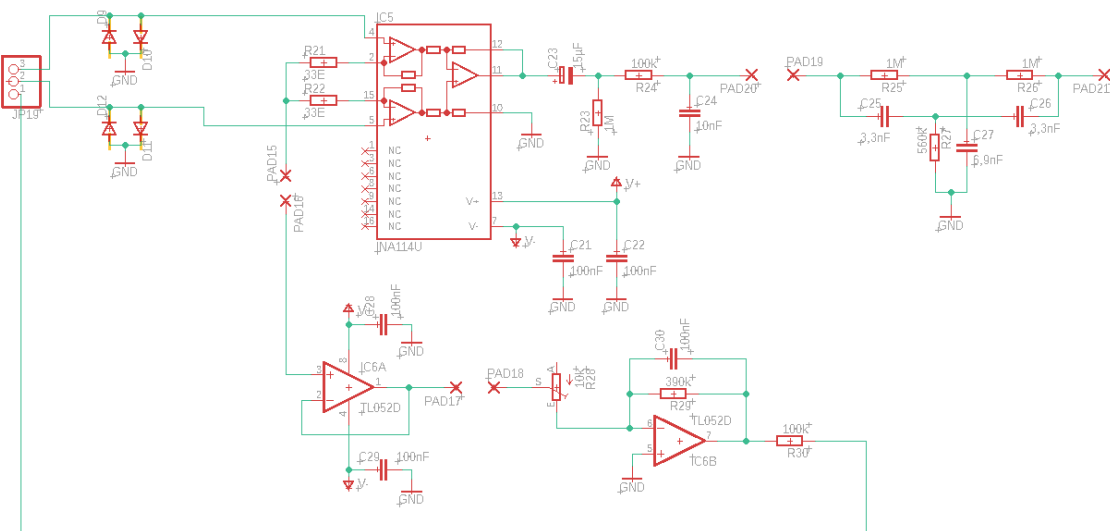


Figure 27: Circuit diagram of the INA115 instrumentation amplifier

An ECG signal has a frequency range of approximately 0.01 Hz to 150 Hz and an amplitude of 0.5 mV to 4 mV. According to the datasheet the gain  $G$  is calculated with eq. (53) [15]

$$G = 1 + \frac{50 \text{ k}\Omega}{R_G} \quad [15] \quad (53)$$

The output voltage range is calculated as follows (see eq. 54).

$$V_O = G * V_D = G * (V_{IN+} - V_{IN-}) \quad [15] \quad (54)$$

$V_O$  ... Output voltage of the instrumentation amplifier

$G$  ... Gain factor

$V_D$  ... Differential voltage of the leads

$V_D$  is calculated by  $V_{IN+} - V_{IN-}$ . In the first derivation according to Einthoven,  $V_{IN+}$  is the left arm and  $V_{IN-}$  is the right arm. In the second Einthoven derivation,  $V_{IN+}$  is the left foot and  $V_{IN-}$  is the right arm. In the third Einthoven derivation,  $V_{IN+}$  is the left foot and  $V_{IN-}$  is the left arm.

### **Dimensioning:**

Equation (55) was used. As the inputs of the microcontroller's ADC can supply or receive a maximum voltage of 3.3 V, the instrumentation amplifier must be dimensioned for a maximum output voltage of 3.3 V.

$$3,3 \text{ V} = G * 0,004 \text{ V} \quad (55)$$

$$G = \frac{3,3 \text{ V}}{0,004 \text{ V}} = 825 \quad (56)$$

$$G = 1 + \frac{50 \text{ k}\Omega}{R_G} \quad (57)$$

$$R_G = \frac{50 \text{ k}\Omega}{G-1} = \frac{50 \text{ k}\Omega}{825-1} = 60,679 \text{ }\Omega \quad (58)$$

$$\frac{R_G}{2} = 30,3398 \text{ }\Omega \quad (59)$$

selected:  $\frac{R_G}{2} = 33 \text{ }\Omega \quad (60)$

- **Driven Right Leg (DRL):**

The Driven Right Leg is used to suppress any common mode interference signals at the input of the instrumentation amplifier. This is done by actively cancelling the interference. To reduce the common mode interference that occurs between the left and right leg, for example, the signal is inverted (using an inverting amplifier) and amplified and fed back to the right leg. A voltage follower is connected between instrumentation amplifier and inverting amplifier (see figure 28).

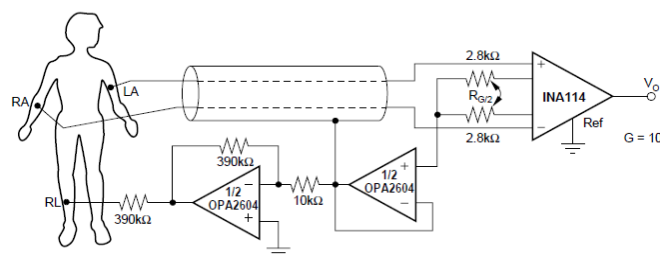


Figure 28: Driven Right Leg from the data sheet [16]

DRL is often used with biological signals to obtain a clean output signal, suppress 50 or 60 Hz interference and improve the CMRR.

### **Dimensioning of the DRL:**

The dimensioning was taken from the INA 114 data sheet [16]. Only the resistance, which is directly connected to the right leg, was reduced to 100 kΩ. This circuit does not contain a leak compensation capacitor (above the resistance in the feedback path of the operational amplifier), as it is used in other typically circuits.

### **Filter:**

Filtering is required to limit all interference above and below the frequency range of the recorded ECG signal (in the typical frequency range of 0.01 - 150 Hz). The filter stages are arranged after the instrumentation amplifier. The notch filter is positioned separately and can be added as an option.

- **High pass:**

The main function of this filter is to allow only frequencies above 0.01 Hz to pass and to remove the DC voltage components (DC offset) that occur.

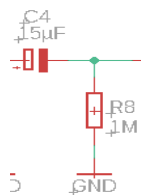


Figure 29: High pass filter

Figure 29 shows the circuit structure of the high-pass filter.

### **Dimensioning:**

$$f_g = \frac{1}{2 * \pi * R * C} \quad (61)$$

The cut-off frequency of the high-pass filter is 0.01 Hz and the resistance R was selected as 1 MΩ. Equation (61) is thus converted for the calculation of capacitor C.

$$C = \frac{1}{2 * \pi * f_g * R} = \frac{1}{2 * \pi * 0,01 \text{ Hz} * 1 \text{ M}\Omega} = 15,915 \text{ nF} \quad (62)$$

A capacitor of 15 nF was selected for the high-pass filter.

- **Low pass filter:**

The main task of the low-pass filter is to suppress frequencies above 150 Hz. Figure 30 shows the low-pass filter.

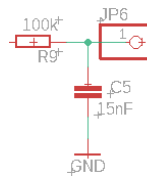


Figure 30: Low pass filter

**Dimensioning:**

The cut-off frequency of the low-pass filter is 150 Hz and a resistance of 100 kΩ was selected. Equation (61) is used and converted for the calculation of the capacitor C.

$$C = \frac{1}{2 * \pi * f_g * R} = \frac{1}{2 * \pi * 150 \text{ Hz} * 100 \text{ k}\Omega} = 15,92 \text{ nF} \quad (63)$$

A capacitor of 15 nF was selected for the low-pass filter.

- **Notch filter:**

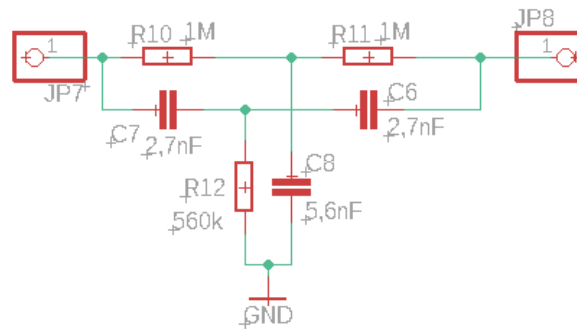


Figure 31: Notch filter

The following paragraph refers to [17].

When working with small biosignals, the interference with the mains voltage can cause problems. A notch filter is used to filter the mains frequency of 50 Hz. The upper T-branch ( $R_{10}$ ,  $R_{11}$  and  $C_8$ ) of the notch filter serves as a low-pass filter. The lower T-branch ( $C_6$ ,  $C_7$  and  $R_{12}$ ) of the notch filter is used as a high-pass filter (see figure 31). The equation (64) can be used to determine the cut-off frequency.

$$f_g = \frac{1}{4 * \pi * R * C} \quad [17] \quad (64)$$

The resistance  $R$  was assumed to be 560 k $\Omega$  and the cut-off frequency should be 50 Hz. Next, the equation (64) was converted so that the capacitance can be calculated.

$$C = \frac{1}{4 * \pi * f_g * R} = \frac{1}{4 * \pi * 50 \text{ Hz} * 560 \text{ k}\Omega} = 2,842 \text{ nF} \quad (65)$$

A capacitance of 2.7 nF was selected.

## 2.6. Supply

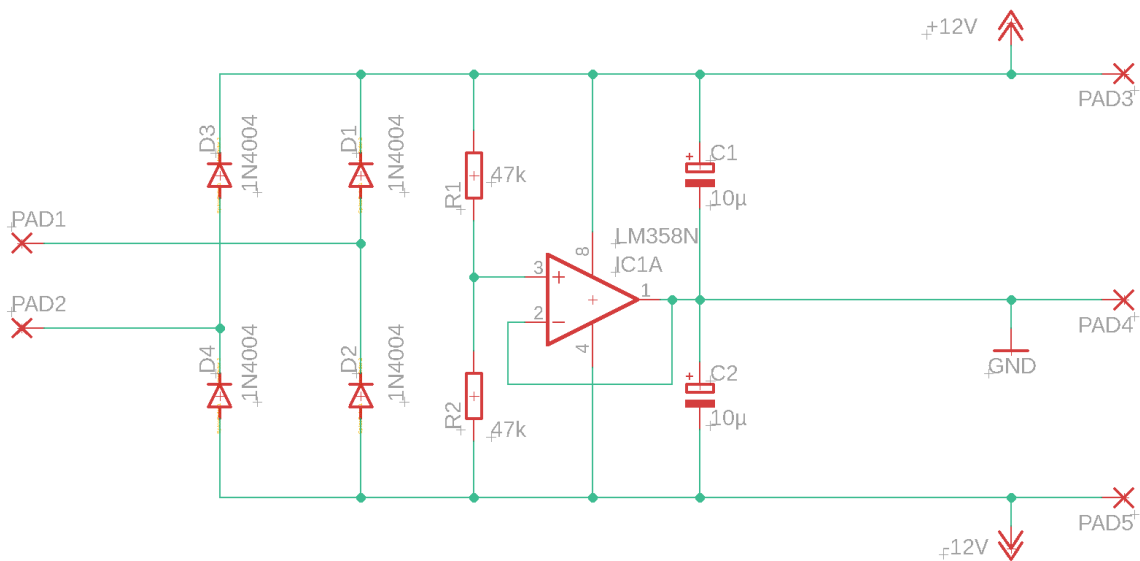


Figure 32: Dual supply circuit with virtual ground [19]

The following paragraph refers to [18,19].

As the system requires a bipolar power supply, the circuit was built as shown in figure 32. The power supply unit has a supply voltage of +24 V and is connected to the input side. The diodes on the input side serve as polarity reversal protection. The circuit consists of a voltage follower, the output voltage of which is set by a resistive voltage divider  $R_1$  and  $R_2$ . As  $R_1 = R_2$ , the output of the OPV yields a voltage of 12 V and serves as signal ground. The signal circuits are therefore fed such that the 24 V and 0 V of the follower circuit serve as the +12 V and -12 V supply rails. The capacitors  $C_1$  and  $C_2$  are used for noise suppression.

A DC voltage offset occurs at the electrodes after a measurement due to the use of the level converter. For preventing electrolysis, a relay switches on the supply voltage of the supply circuit at the start of a measurement. After the measurement, the relay opens again and the circuit, including the level converter, is no longer supplied with the supply voltage. Figure 33 shows the relay circuit.

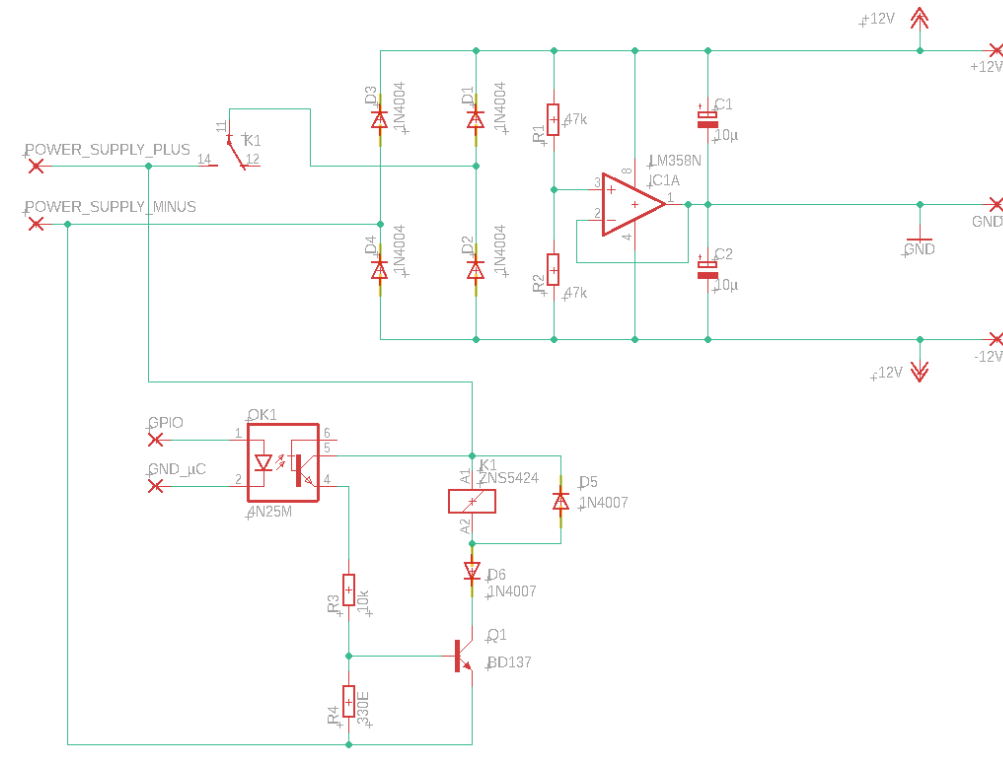


Figure 33: Supply circuit with switching relay

The GPIO PC1 is connected to the anode of the optocoupler OK1 and the ground of the microcontroller is connected to the cathode. When the programme is executed, the first GPIO is set to logic 1, which corresponds to 3.3 V and activates the optocoupler diode. This turns on the transistor of the optocoupler and also the transistor Q1 in figure 33. The two resistors form a voltage divider so that a base-emitter voltage of 0.7 V is applied (see eq. 66 - 68). This switches the relay through and the circuit board of the supply circuit is supplied. As soon as the measurement sequence is completed, the GPIO pin is set back to logic 0, the relay opens again and the supply circuit is no longer supplied.

$$\frac{U_{BE}}{U_{Supply}} = \frac{R_4}{R_3 + R_4} \quad (66)$$

$$U_{BE} = U_{Supply} * \frac{R_4}{R_3 + R_4} \quad (67)$$

$$U_{BE} = 24 V * \frac{330 \Omega}{10 k\Omega + 330 \Omega} = 0,766 V \quad (68)$$

## 2.7. Electrodes

The current signals are defined as input variables of the system and the voltage signals at the thorax phantom are defined as output variables. The electrolyte in the thorax phantom and the injected current form a circuit. The electrolyte, as mentioned in the introduction, is a 0.9% NaCl solution. Figure 34 below shows the equivalent circuit diagram of the electrode-electrolyte junction.

Figure 34 redrawn and modified from [20].

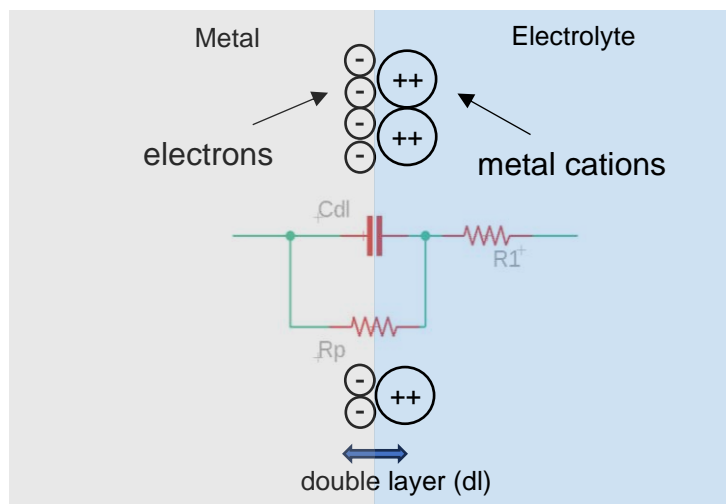


Figure 34: Equivalent circuit diagram electrode-electrolyte junction [20]

The following paragraph refers to [20].

$R_1$  is assumed to be the electrical resistance of the electrolyte (including supply line and electrode). With alternating current, the double layer behaves like a capacitor  $C_{dl}$  and a resistance  $R_p$  (polarisation resistance or contact resistance) act in parallel at the interface, which represents the activation energy of the redox reaction. The components mentioned above are measured by means of impedance spectroscopy. Voltammetry is also measured. The Palmsense 3 (PalmSens B.V.) programme PSTrace from PalmSens (PalmSens B.V.) was used for this measurement. The aim is to obtain electrodes with a low impedance in the frequency range of the ECG and to select appropriate materials.



- **Electrochemical impedance spectroscopy (EIS):**

This subitem refers to [21,22 p.102,23].

At the transition from electrode to electrolyte, electrons recombine with cations in a Redox-reaction and hence establish an electrical current by charge transfer. Electrochemical processes occur at the boundary layer that strongly influence the current flow. Electroimpedance spectroscopy (EIS) is used to determine the frequency dependence of the current flow. With this method, the electrode-electrolyte impedance can be determined using a frequency spectrum. At a constant voltage (potentiostatic method) or constant current (galvanostatic method), an alternating voltage or alternating current with a small amplitude is superimposed at one point and the phase shift between voltage and current is measured. By signal multiplication of a sine and cosine signal and averaging, the useful signal is separated from harmonics, noise and direct current components (see figure 35). The magnitude of the complex resistance and the phase are determined using a frequency response analyser. In impedance spectroscopy, measurements are taken from very high to very low frequencies.

Figure 35 redrawn and modified from [22 p.102].

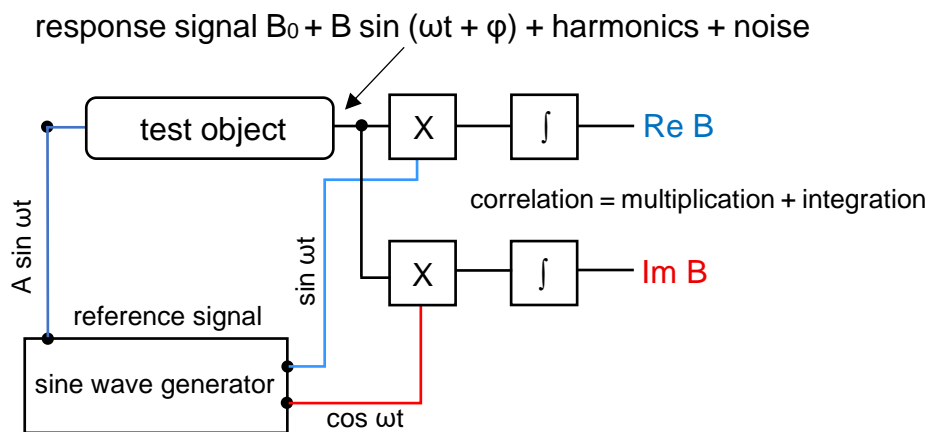


Figure 35: Structure of a frequency response analyser [22 p.102]

**Measurement setup:**

The measurement setup is shown in figure 36. During the measurement, a controllable potential is applied to the electrode and the current flowing through the electrode is measured. The reaction takes place at the working electrode (WE). In

this application, the materials to be analysed that can be considered as possible electrodes are referred to as WE. A silver-silver chloride electrode is used as a (RE), which is kept at a constant potential and thus keeps the system stable. If a reaction takes place that releases a charge, an electric current can flow. However, a reaction usually only takes place above a certain potential difference across the interface, as the activation energy can then be supplied. This changes the environment of the electrode and therefore also the potential. Fluctuations in the potential lead to fluctuations in the current. The reference electrode should measure the potential at a defined point and pass it on to a control circuit, which ensures that the reference potential remains constant by varying the voltage between the working electrode and the counter electrode. The counter electrode (CE) consists of an inert type of metal or a carbon electrode. Platinum is well suited as a counter electrode due to its very good inert properties. The counter electrode should not influence the working electrode and should not limit the current. Furthermore, the counter electrode should not limit the current or influence the WE [33].

The materials compared are brass, chrome-plated brass, stainless steel, gold-plated stainless steel and silver-silver chloride.

Figure 36 redrawn and modified from [14].

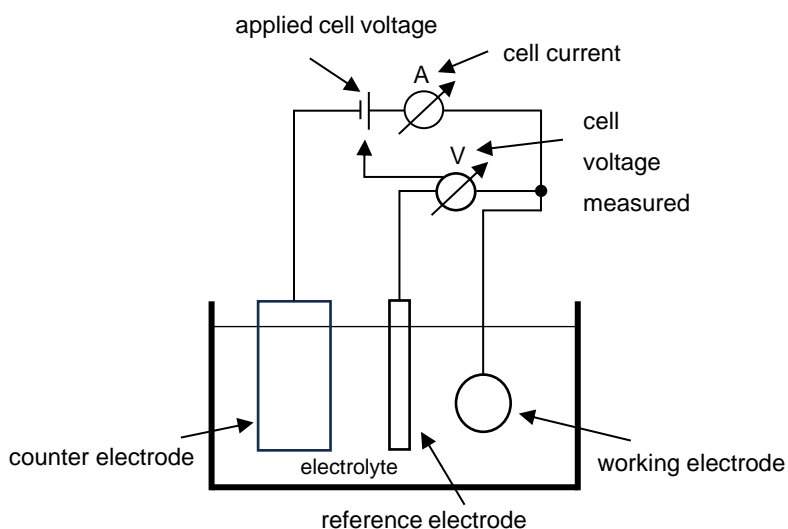


Figure 36: Measurement setup for impedance spectroscopy and voltammetry [14]

The parameters set for impedance spectroscopy can be seen in figure 37.

Measurement Info Reference electrode

Technique: Impedance Spectroscopy ?

Sample: Identification of a Reversible, Quasi-Reversible, or ....

Sensor:

Current range:

100 pA 1 nA 10 nA 100 nA 1  $\mu$ A 10  $\mu$ A 100  $\mu$ A 1 mA 10 mA

— Pretreatment settings

E condition 1: 0.0 V

t condition 1: 0 s

E condition 2: 0.0 V

t condition 2: 0 s

— Impedance Spectroscopy settings

t equilibration: 8 s

Scan type: FixedPotential

E dc: 0.0 V

E ac: 0.25 V

Frequency type: Scan

☒ Pretreat each frequency

n frequencies: 150 list

Max. frequency: 10000.0 Hz

Min. frequency: 0.1 Hz

t Min. sampling: 0.01 s

t Max. equilibration: 1.0 s

☒ Measure OCP

\*\*\*

+ Advanced settings

— Post measurement

☒ Cell on after measurement

Figure 37: Parameter settings for impedance spectroscopy

The "Pretreatment settings" are all set to zero. No DC voltages are applied, only AC voltage at 0.25 V. The frequency range of the measurement is between 0.1 Hz and 10 kHz with 150 measuring points.

- **Cyclic voltammetry:**

This subitem refers to [24].

In cyclic voltammetry, a potential is applied and the current is measured. The potential increases or decreases linearly. The change in potential ( $\partial E$ ) per time is the scan rate  $v$  (see eq. 69).  $E$  is a voltage.

$$v = \frac{\partial E}{\partial t} \quad (69)$$

At the beginning of the measurement, the potential is in a range where no electrochemical reaction is taking place. The linear sweep of the potential is selected in a way that the potential crosses the formal potential of the analysed object (see figure 38).  $E_{\text{vertex1}}$  stands for the lower vertex potential and  $E_{\text{vertex2}}$  for the upper vertex potential.

Figure 38 redrawn and modified from [24].

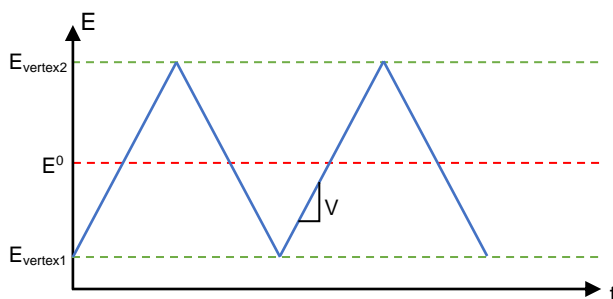


Figure 38: Cyclic voltammetry [24]

A cycle is completed when the starting potential has been reached. This process can be repeated. This allows the impedance to be calculated by reading the voltage and current difference, but only if the curve is linear.

The measurement setup is the same as in section 2.7.1. The voltammetry parameters set can be seen in figure 39.

Measurement Peaks Info Reference electrode

Technique: Cyclic Voltammetry ?

Sample: Identification of a Reversible, Quasi-Reversible, or ...

Sensor:

Current range:

100 pA 1 nA 10 nA 100 nA 1 uA 10 uA 100 uA 1 mA 10 mA

— Pretreatment settings

E condition: 0.0 V

t condition: 0 s

E deposition: 0.0 V

t deposition: 0 s

— Cyclic Voltammetry settings

t equilibration: 8 s

E begin: 0.0 V

E vertex1: 0.5 V

E vertex2: -0.5 V

E step: 0.01 V

Scan rate: 0.1 V/s

Number of scans: 5

— Post measurement

☐ Cell on after measurement

— Auxiliary measurement

☐ Aux. input

Figure 39: Voltammetry parameters set

The initial voltage is 0 V, rises to 0.5 V and falls to -0.5 V. The scan rate is 0.1 V/s.

The following materials were investigated with regard to their electrochemical behaviour in NaCl solution.

- Brass
- Chrome- plated brass
- Stainless steel
- Stainless steel- gold- plated
- Silver- Silver chloride (Ag/AgCl)

a. Brass:

The electrodes originally used were made of brass, there for they can be used as a reference. Brass is suitable because the brass-NaCl interface has a low transfer resistance. The disadvantage of brass is that an oxide layer forms on the surface after a certain time, which reduces conductivity. For this reason, brass will be not used as an electrode. The measurement results can be seen in selection 3.5.

b. Chrome- plated brass:

One idea was to use chrome-plated brass balls. One advantage over the brass spheres would be that no oxide layer could form on the surface of the sphere and this would not impair the conductivity. A redox reaction took place, but the voltammetry was asymmetrical. The measurement results can be seen in selection 3.5.

c. Stainless steel:

Next, stainless steel balls were used. One advantage over the brass spheres would be that no oxide layer can form on the surface of the spheres and therefore the conductivity would not deteriorate. Unfortunately, however, no effective redox reaction took place, which means that the transfer resistance is very high. The measurement results can be seen in selection 3.5.

d. Stainless steel- gold- plated:

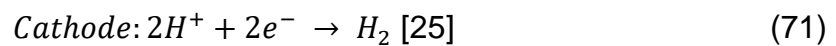
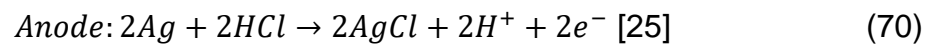
The gold-plated stainless steel spheres had the same problem as the stainless steel spheres. The measurement results can be seen in selection 3.5.

e. Silver- Silver chloride (Ag/AgCl):

This subitem refers to the quote [25].

Ag/AgCl electrodes were then tested. The disposable electrode was placed in the electrolyte and a reaction occurred and according to voltametry the impedance is quite low. In the next step, silver spheres were ordered, drilled and chlorinated using an HCl solution. A silver wire was used as a counter electrode. Chlorination is carried out using an HCl solution by immersing the silver ball and a silver wire and applying a DC voltage of 1-2 volts and switching off the current limiter. The silver ball is connected to the positive pole and the silver wire to the negative pole of the power supply unit. This creates a silver chloride layer on the silver ball. The duration of chlorination is 20 to 300 seconds.

The reaction equation is:



The measurement results can be seen in selection 3.5.

## 2.8. Determination of the conductivity of the NaCl solution

As in selection 1, a thorax phantom filled with physiological or 0.9% saline solution should be used for the laboratory exercise. The following constants are required to calculate the conductivity.

- Atomic mass of sodium (Na) = 22,9897 u [29]
- Atomic mass of chloride (Cl) = 35,453 u [30]
- Molar conductivity NaCl  $\Lambda = 126,5 \text{ S cm}^2 / \text{mol}$  [31]
- Equation of the concentration of substances

$$c = \frac{n}{V} \text{ [32]} \quad (72)$$

where n is the amount of substance and V is the volume

- specific conductivity

$$\kappa = c * \Lambda \text{ [31]} \quad (73)$$

The following equations were used to determine the conductivity of the physiological saline solution:

$$\text{Sum of the atomic mass NaCl} = 22,98 + 35,45 = 58,44 \text{ u} = 58,44 \frac{\text{g}}{\text{mol}} \quad (74)$$

$$\text{Amount of substance: } 0,9 \% \text{ NaCl} = 9 \frac{\text{g}}{1000 \text{ ml}} = 9 \frac{\text{g}}{\text{l}} \quad (75)$$

$$c = \frac{9 \frac{\text{g}}{\text{l}}}{58,44 \frac{\text{g}}{\text{mol}}} = 0,15 \frac{\text{mol}}{\text{l}} \quad (76)$$

$$\begin{aligned} \text{Specific conductivity } \kappa &= c * \Lambda = 0,15 \frac{\text{mol}}{\text{l}} * 126,5 \frac{\text{S cm}^2}{\text{mol}} = 0,15 \frac{\text{mol}}{1000 \text{ cm}^3} * \\ 126,5 \frac{\text{S cm}^2}{\text{mol}} &= 0,01948 \frac{\text{S}}{\text{cm}} = 19,48 \frac{\text{mS}}{\text{cm}} \end{aligned} \quad (77)$$

The saline solution requires a specific conductivity of 19.48 mS / cm.

Before the tank was filled with water, the height at which the electrodes should be positioned, was measured. The height at which the electrodes should be positioned is



approximately 27 cm and was measured from the bottom of the tank to the centre of the cross [21].

The tank was then filled with water, salt was gradually added and stirred with a long stick until the salt had dissolved.

The conductivity was then measured using the digimeter L 21 conductivity meter (AQUALYTIC, Dortmund, Germany) (see figure 40).



Figure 40: Instrument for the conductivity of the electrolyte

## 3. Results

### 3.1. Howland current source

The measurements were carried out with the RIGOL DS1204B oscilloscope. All three Howland sources were tested for their limits. During the first measurement of the Howland source, the load up to which the source can be loaded was tested. In this measurement (using the frequency generator type: FeelElec DDS Function/Arbitrary Waveform Generator FE FY6900, manufacturer FeelTech/FeelElec Zhengzhou Feiyi Technology Co., Ltd.), the input frequency was 1 Hz and the input voltage was 3.3 V<sub>pp</sub>.

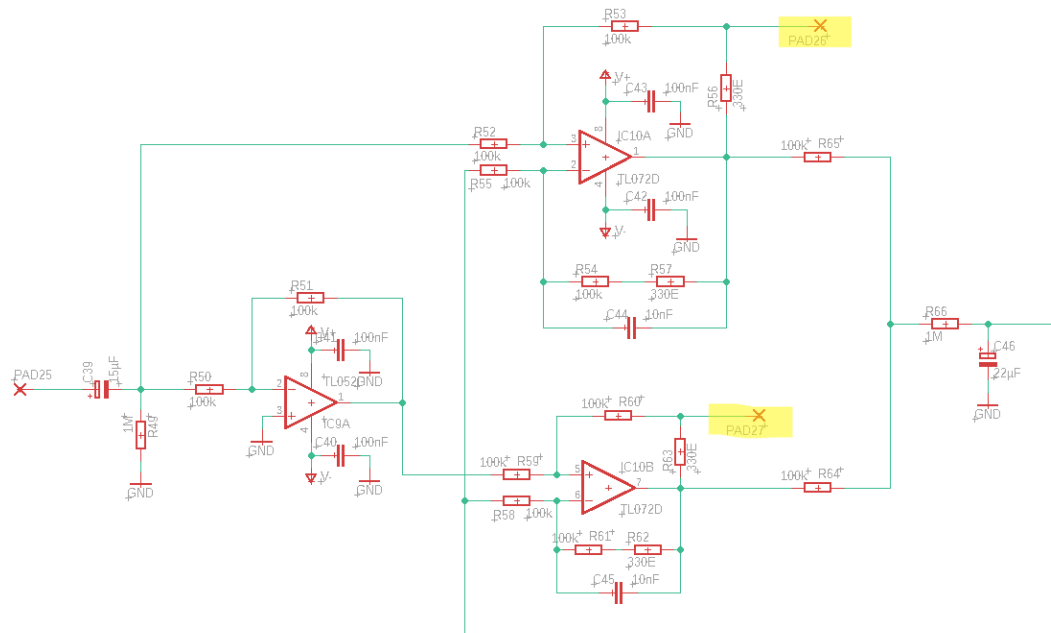


Figure 41: Circuit diagram of the first Howland current source

Table 1: Measurement results of the first Howland current source

R	CH1 (Pad 26 in figure 43)	CH2 (Pad 27 in figure 43)	CH1 – CH2	$I = (CH1 - CH2) / R$ calculated)
10 $\Omega$	55 mV <sub>pp</sub>	70 mV <sub>pp</sub>	120 mV <sub>pp</sub>	12 mA <sub>pp</sub>
39 $\Omega$	190 mV <sub>pp</sub>	200 mV <sub>pp</sub>	380 mV <sub>pp</sub>	9,74 mA <sub>pp</sub>
100 $\Omega$	480 mV <sub>pp</sub>	490 mV <sub>pp</sub>	960 mV <sub>pp</sub>	9,6 mA <sub>pp</sub>
220 $\Omega$	1,1 V <sub>pp</sub>	1,1 V <sub>pp</sub>	2,2 V <sub>pp</sub>	10 mA <sub>pp</sub>
560 $\Omega$	2,75 V <sub>pp</sub>	2,75 V <sub>pp</sub>	5,5 V <sub>pp</sub>	9,82 mA <sub>pp</sub>
1 k $\Omega$	4,8 V <sub>pp</sub>	4,8 V <sub>pp</sub>	9,6 V <sub>pp</sub>	9,6 mA <sub>pp</sub>
2,2 k $\Omega$	■			

■ ... Saturation

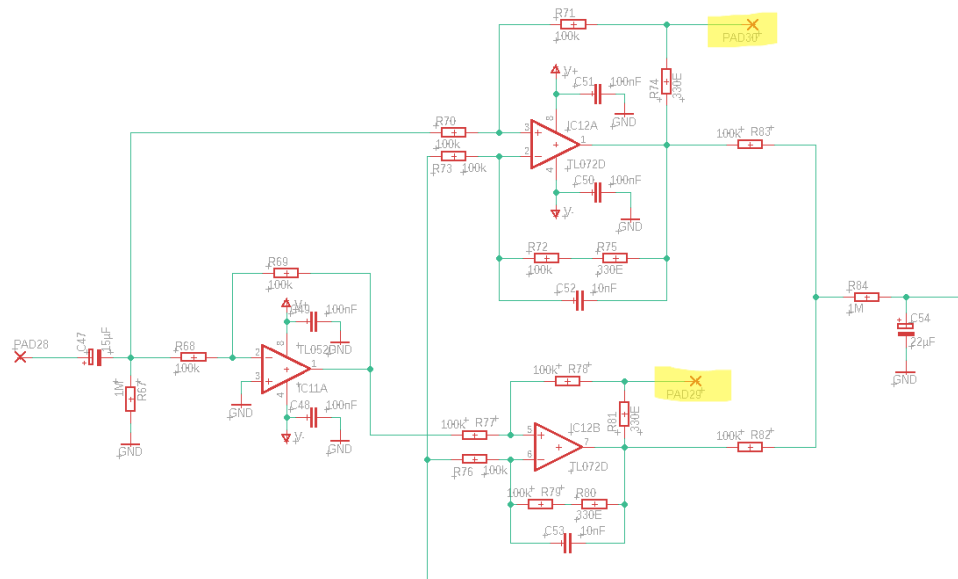


Figure 42: Circuit diagram of the second Howland current source

Table 2: Measurement results of the second Howland current source

R	CH1 (Pad 30 in figure 44)	CH2 (Pad 29 in figure 44)	CH1 – CH2	$I (= (CH1 - CH2) / R \text{ calculated})$
10 $\Omega$	60 mV <sub>pp</sub>	65 mV <sub>pp</sub>	100 mV <sub>pp</sub>	10 mA <sub>pp</sub>
39 $\Omega$	190 mV <sub>pp</sub>	200 mV <sub>pp</sub>	380 mV <sub>pp</sub>	9,74 mA <sub>pp</sub>
100 $\Omega$	490 mV <sub>pp</sub>	480 mV <sub>pp</sub>	960 mV <sub>pp</sub>	9,6 mA <sub>pp</sub>
220 $\Omega$	1,1 V <sub>pp</sub>	1,1 V <sub>pp</sub>	2,2 V <sub>pp</sub>	10 mA <sub>pp</sub>
560 $\Omega$	2,8 V <sub>pp</sub>	2,8 V <sub>pp</sub>	5,6 V <sub>pp</sub>	10 mA <sub>pp</sub>
1 k $\Omega$	4,8 V <sub>pp</sub>	4,8 V <sub>pp</sub>	9,6 V <sub>pp</sub>	9,6 mA <sub>pp</sub>
2,2 k $\Omega$	■			

■ ... Saturation

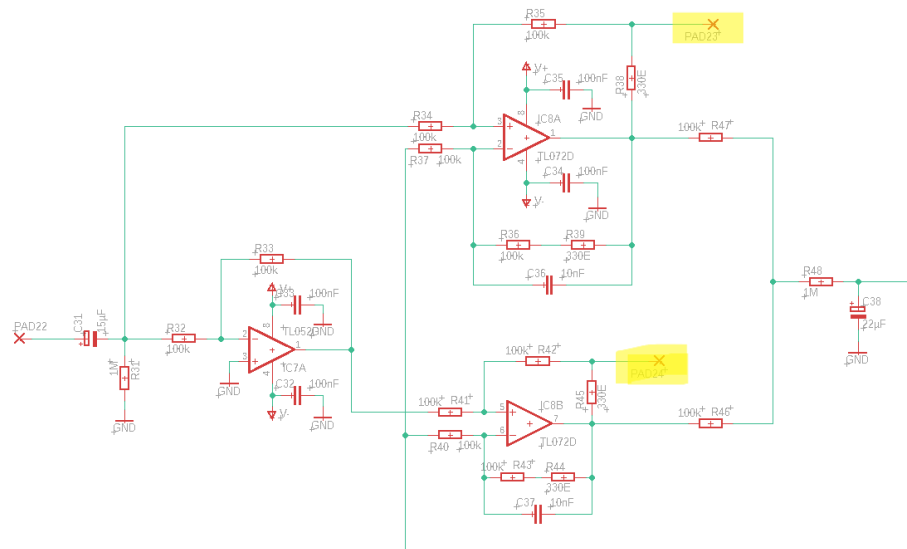


Figure 43: Circuit diagram of the third Howland current source

Table 3: Measurement results of the third Howland current source

R	CH1 (Pad 26 in figure 45)	CH2 (Pad 26 in figure 45)	CH1 – CH2	I (= (CH1 – CH2) / R calculated)
10 Ω	60 mV <sub>pp</sub>	60 mV <sub>pp</sub>	100 mV <sub>pp</sub>	10 mA <sub>pp</sub>
39 Ω	190 mV <sub>pp</sub>	200 mV <sub>pp</sub>	380 mV <sub>pp</sub>	9,74 mA <sub>pp</sub>
100 Ω	480 mV <sub>pp</sub>	480 mV <sub>pp</sub>	960 mV <sub>pp</sub>	9,6 mA <sub>pp</sub>
220 Ω	1,1 V <sub>pp</sub>	1,1 V <sub>pp</sub>	2,2 V <sub>pp</sub>	10 mA <sub>pp</sub>
560 Ω	2,8 V <sub>pp</sub>	2,8 V <sub>pp</sub>	5,6 V <sub>pp</sub>	10 mA <sub>pp</sub>
1 kΩ	4,8 V <sub>pp</sub>	4,8 V <sub>pp</sub>	9,6 V <sub>pp</sub>	9,6 mA <sub>pp</sub>
2,2 kΩ	■			

- ... Saturation

As can be seen from the measurement results, the Howland sources are stable up to a load of 1k $\Omega$  and supply a current of 10 mA  $\pm$  0.93 mA. This is perfectly adequate for this application, as the electrode should only have a low impedance. The total voltage (Math column in table 1, 2 and 3) is used to calculate the current and is divided by the corresponding resistance value. As can be seen from tables 1, 2 and 3, the current is

constant. The Howland sources therefore supply a constant current until their limit has been reached.

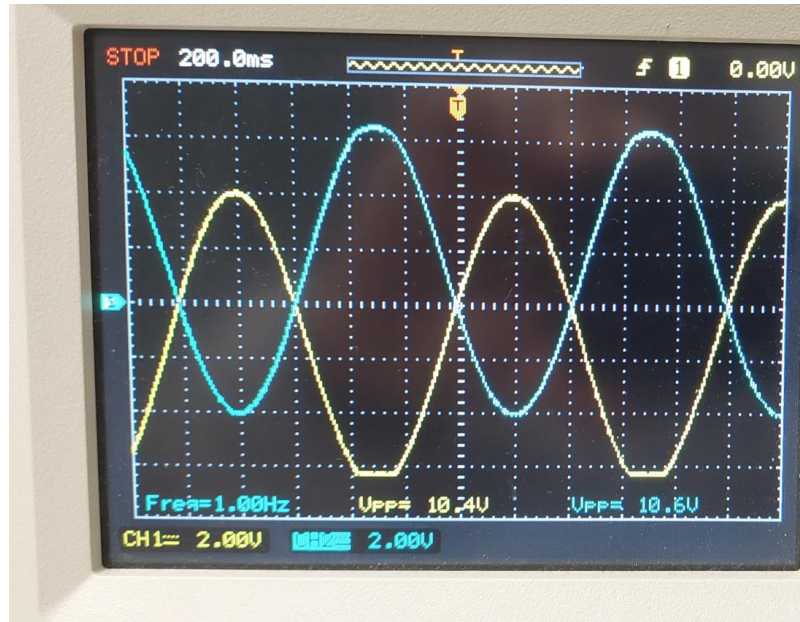


Figure 44: Howland current source at a load of 2,2 k $\Omega$

As can be seen in figure 44, the operational amplifier saturates at a load of 2.2 k $\Omega$  (signal peaks are cut off) and the two signals are offset from each other. The mean value of the signals shifts towards the operating voltage, resulting in a non-zero mean value. It is noticeable that the shift of the mean value and the saturation start at the same time. No explanation could be found as to why this phenomenon occurs.

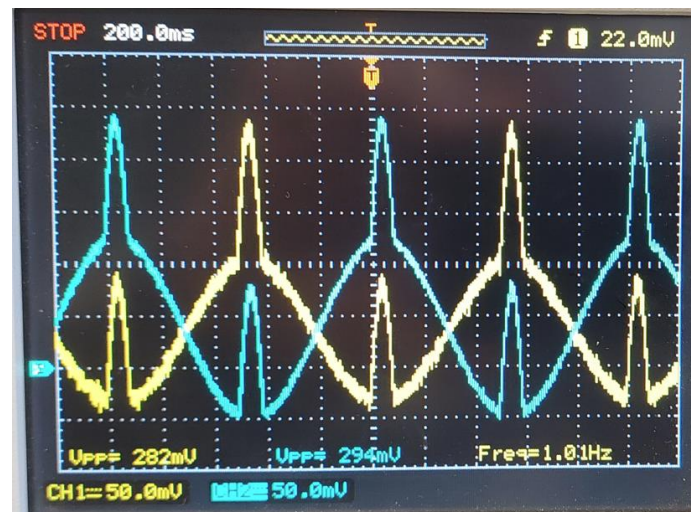


Figure 45: Measurement at  $10\ \Omega$  and  $11\ V_{pp}$

Figure 45 shows that the signal shape is lost, which is typical when a circuit enters saturation. The source and sink become saturated at  $10\ \Omega$  and  $11\ V_{pp}$ .

As mentioned in selection 2.4, the compression point was also determined. The compression point was determined out at frequencies of 1 Hz, 10 Hz, 20 Hz, 50 Hz and 100 Hz at a load of  $18\ \Omega$ . The input voltage is slowly increased from  $0\ V_{pp}$  to  $11\ V_{pp}$  in  $0,5\ V_{pp}$  steps using a frequency generator (type: Feel Elec DDS Function/Arbitrary Waveform Generaator FE FY6900) and the current is measured using a multimeter (type: TE.ELECTRONIC MS8264).

The load current is calculated using eg. (53) from selection 2.4. The tables can be found in the appendix.

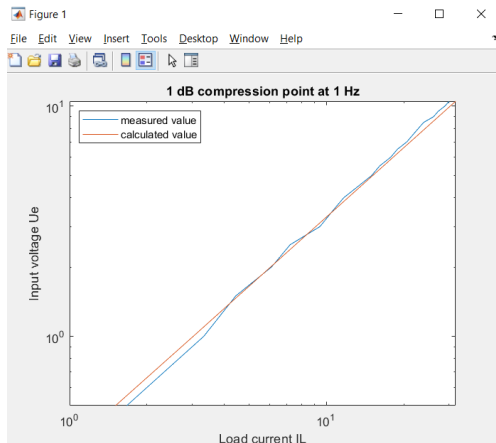


Figure 46: Compression measurement  
at 1 Hz

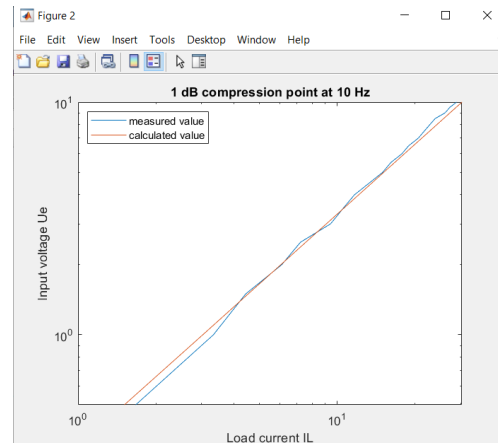


Figure 47: Compression measurement  
at 10 Hz

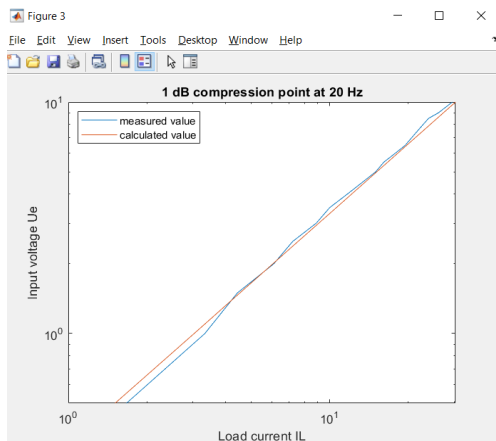


Figure 48: Compression measurement  
at 20 Hz

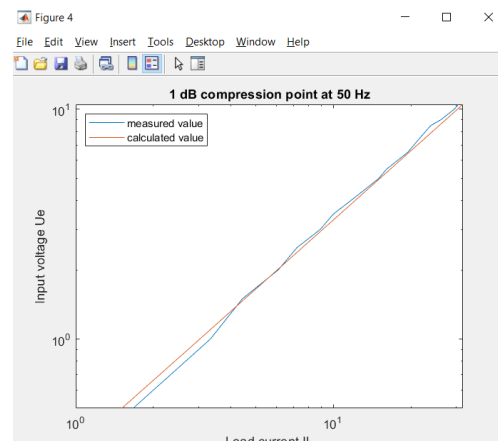


Figure 49: Compression measurement  
at 50 Hz

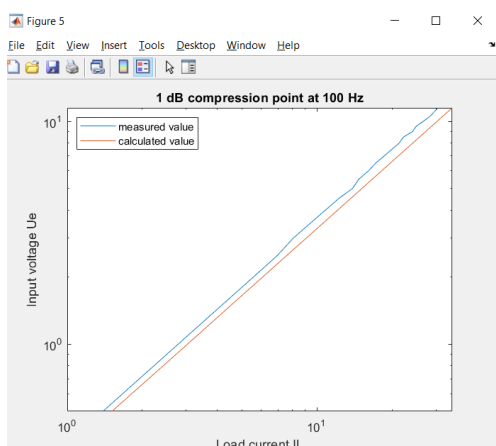


Figure 50: Compression measurement  
at 100 Hz

As can be seen in figures 46, 47, 48, 49 and 50, there is no 1 dB kink, so the system is very stable in the low-frequency range.



### 3.2. Instrumentation amplifier

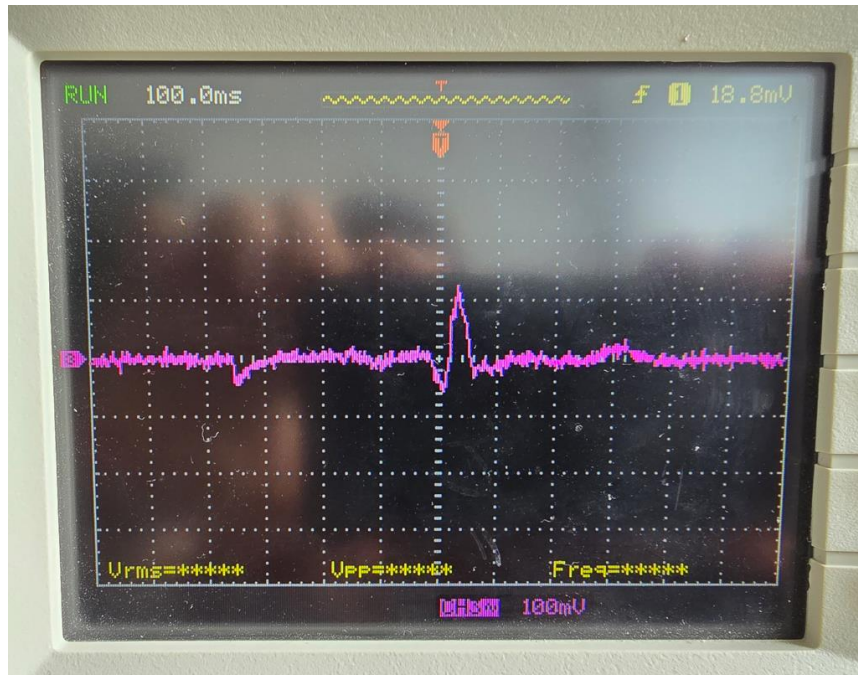


Figure 51: Measurement of the Einthoven lead 3 with noise component

During the first measurements, it was noticed that the signal has a noise component (see figure 51). In the next step, two frequency generators with the same frequency and a voltage difference of 0.04 V were connected to the inputs of the instrumentation amplifier. The reason for testing the instrumentation amplifier with a function generator was to determine the gain of the instrumentation amplifier was sufficient and whether there was less noise when a function generator (which is a noise source) was connected. The result was that the noise was at the expected level. The thorax phantom thus represents a certain input impedance and a coupling element for coupled interference voltages. Next, a high-pass filter with a cut-off frequency of 0.01 Hz was attached to the amplifier's inputs to suppress any out-of-band interference in advance. As the ADC of the microcontroller cannot process negative voltages, a pull-up resistor of 100 k $\Omega$  was installed at the output of the low-pass filter and supplied with 3.3 V (from the microcontroller). This raises the zero line of the received ECG signal to 1.65 V.



Figure 52: Measurement of the Einthoven lead 1



Figure 53: Measurement of the Einthoven lead 2



Figure 54: Measurement of the Einthoven lead 3

As can be seen in figures 52, 53 and 54, the instrumentation amplifiers function and can reproduce the ECG signal.

### 3.3. Electrodes

Figure 55 shows the electrochemical impedance spectrum of an Ag/AgCl electrode. Unfortunately, the axes are scaled differently, therefore the theoretical semi-arc is deformed towards an ellipse. Moreover, the typical 'diffusion tail' which is seen in many electrode spectra is not present. Impedance spectroscopy is a small-signal analysis and only applies to linearised parts at the operating point of the electrode. Whereas voltammetry shows the complete non-linearity of the electrode and therefore the complete behaviour of the electrode, asymmetries can be shown using voltammetry. Voltammetry is a large-signal analysis. Since large signals are applied via the electrodes, these should be linear over the entire dynamic range, and this is better visualised by voltammetry than by impedance spectroscopy.

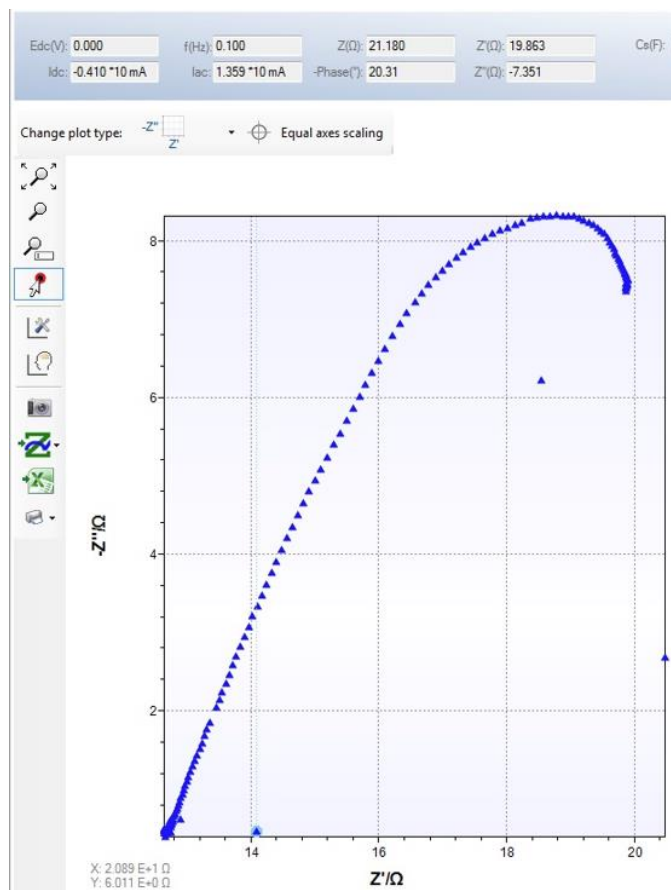


Figure 55: Electrochemical impedance spectroscopy of an Ag/AgCl electrode

In cyclic voltammetry, the impedance is calculated from the voltage and current difference, as follows:

$$Z = \frac{\Delta V}{\Delta I} \quad (78)$$

- **Brass:**

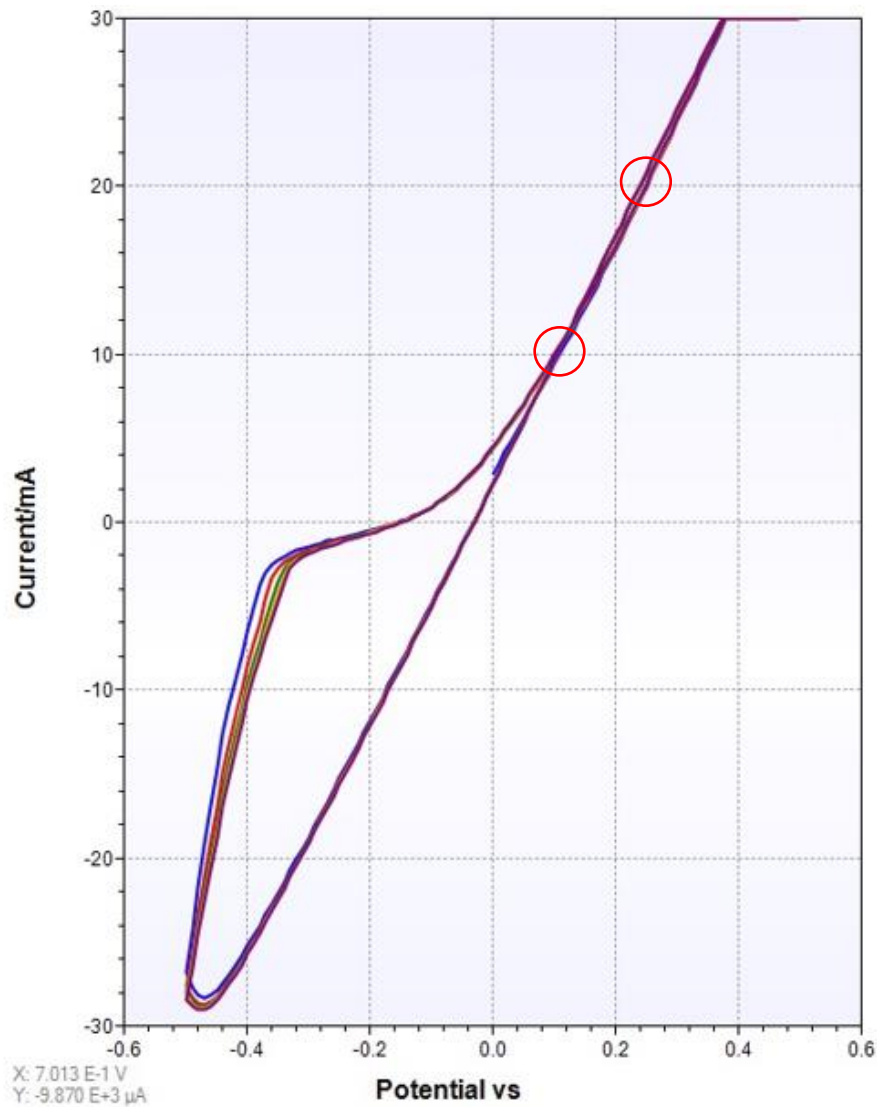


Figure 56: Voltammetry measurement of the brass sphere

Two red points have been marked in figure 56. The points for determining the impedance were selected because the Howland source is limited to 10 mA. The second point was selected at the double overload limit, because it can also be shown here that the sphere can work well in this area. No selection can be made in the negative range because the hysteresis range is in effect. Zero mA cannot be selected either, because the hysteresis is already beginning. For the voltage and current difference and the  $\Delta I$  is 10 mA and the  $\Delta V$  is 0.14 V. This results in an impedance of 14  $\Omega$  according to equation (78). The reaction is not completely



reversible (asymmetrical) and therefore has a nonlinear behaviour. The brass electrodes are only used as a reference. For this reason, no impedance spectroscopy was carried out.

- **Chrome-plated brass:**

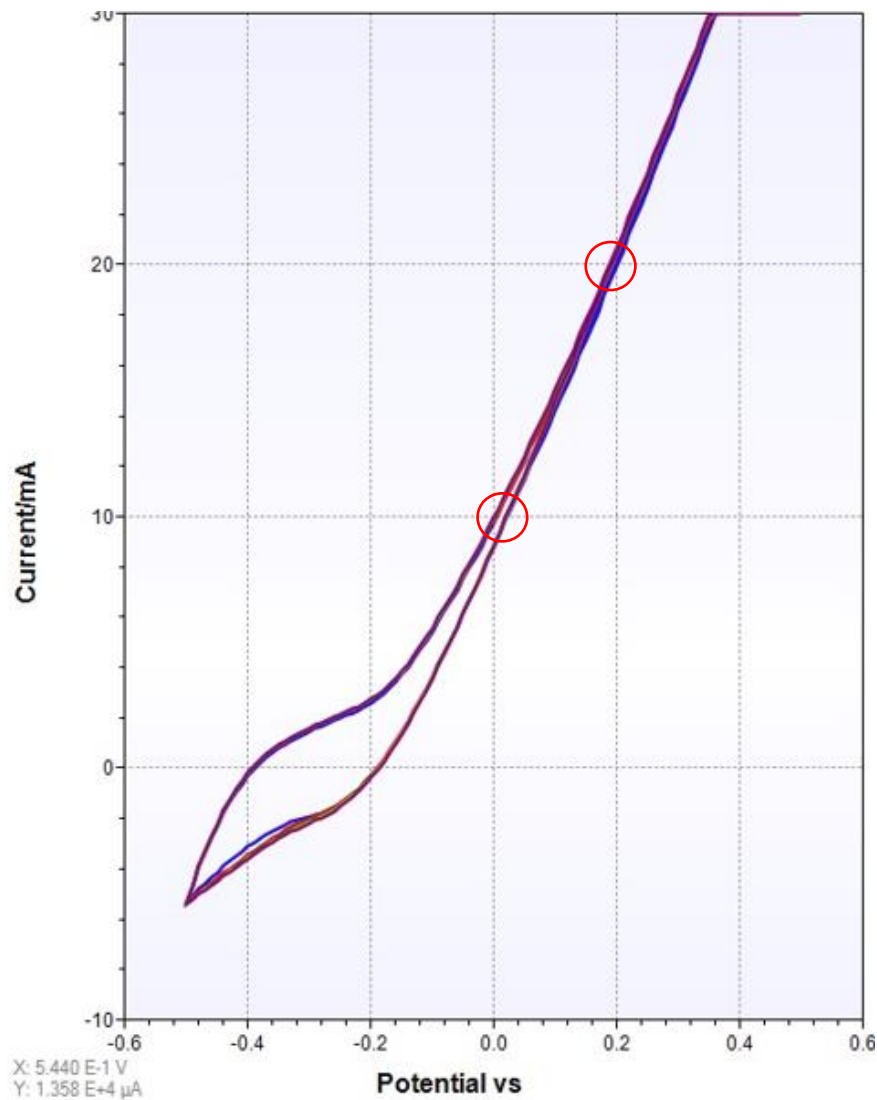


Figure 57: Voltammetry measurement of the brass chrome-plated sphere

Two red points have been marked in figure 57. The points for determining the impedance were selected because the Howland source is limited to 10 mA. The second point was selected at the double overload limit, because it can also be shown here that the sphere can work well in this area. No selection can be made in the negative range because the hysteresis range is in effect. Zero mA cannot be

selected either, because the hysteresis is already beginning. For the voltage and current difference and the  $\Delta I$  is 10 mA and the  $\Delta V$  is 0.2 V. This results in an impedance of 20  $\Omega$  according to equation (78). The reaction is not completely reversible (asymmetrical) and therefore has a nonlinear behaviour. For this reason, no impedance spectroscopy was carried out.

- **Stainless steel:**

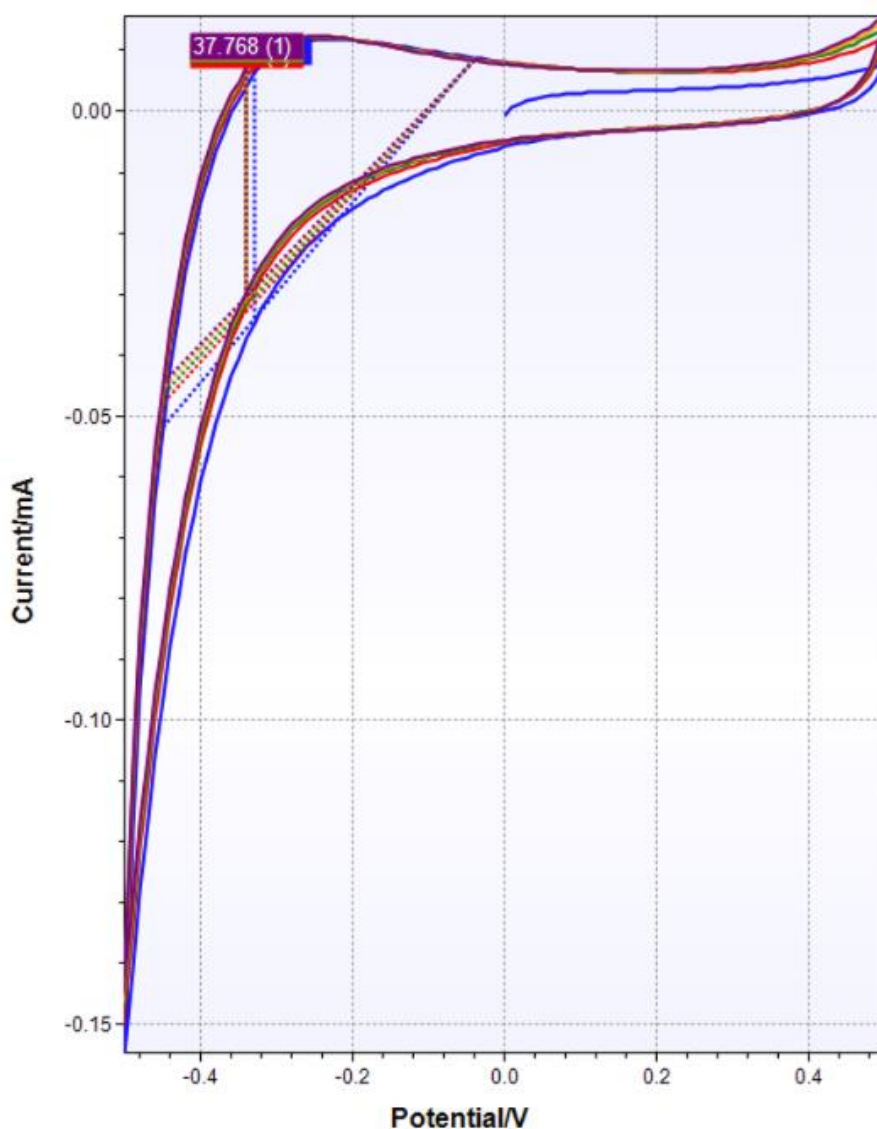


Figure 58: Voltammetry measurement of the stainless steel sphere

With the stainless steel sphere (see figure 58), you can see that the curve is flat and the impedance is quite high. Therefore, the stainless steel sphere is not usable.

- Stainless steel - gold-plated:

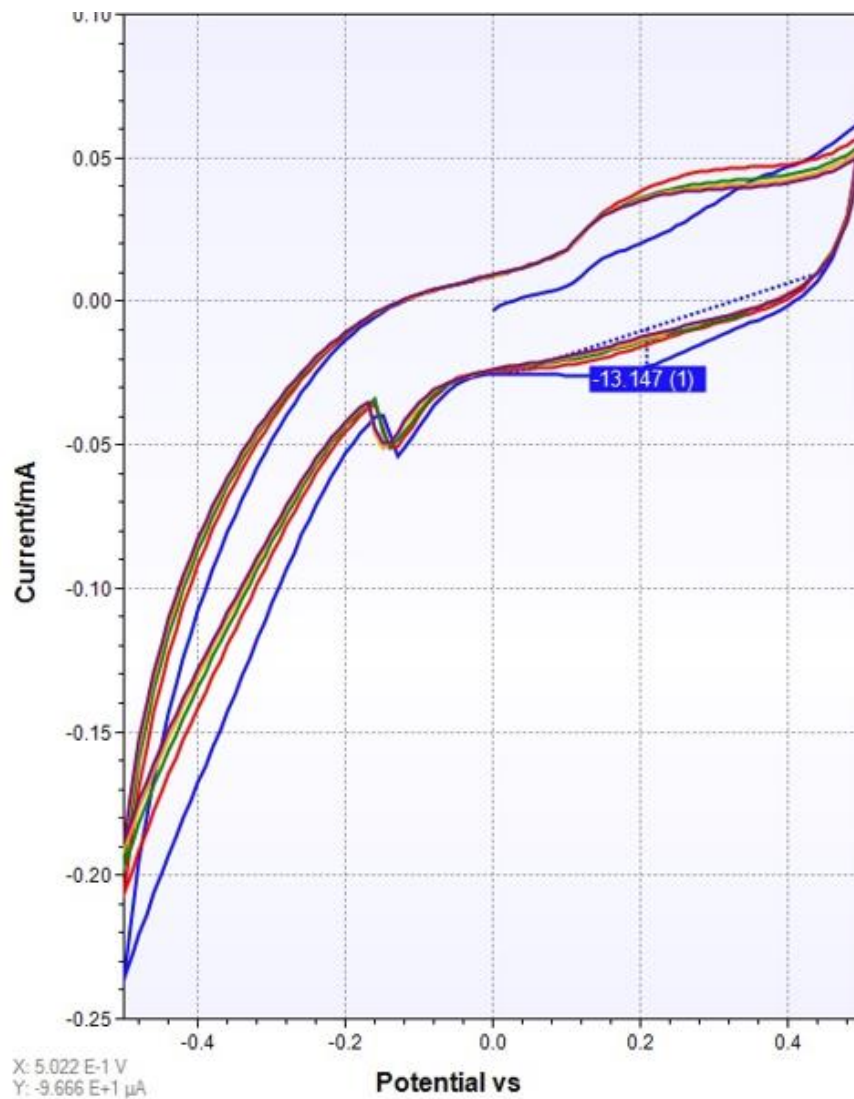


Figure 59: Voltammetry measurement of the stainless steel gold-plated sphere

It can also be seen with the stainless steel gold-plated sphere (see figure 59) that the curve is not a straight line and the impedance is also high here. The stainless steel sphere is therefore not usable.



- Silver-silver chloride (Ag/AgCl):

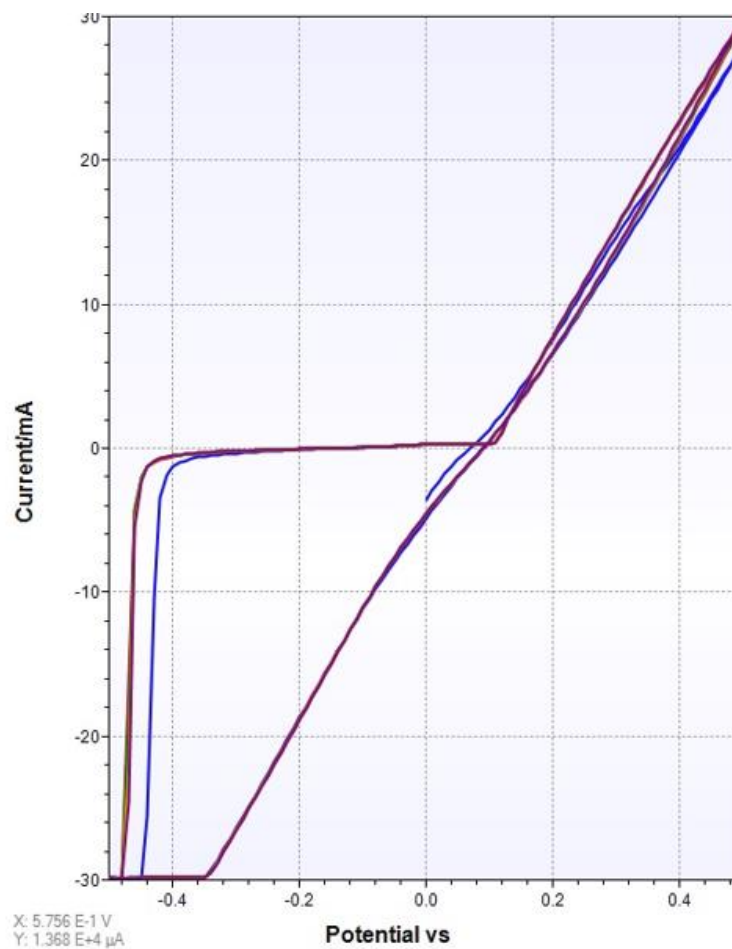


Figure 60: Voltammetry measurement of the own silver-silver chloride sphere

Figure 60 shows that the hysteresis is quite pronounced. For this reason, the programme settings have been changed (see figure 61).

The screenshot shows the 'Voltammetry.psmethod' window with the following settings:

- Measurement:** Peaks, Info, Reference electrode
- Technique:** Cyclic Voltammetry
- Sample:** Identification of a Reversible, Quasi-Reversible, or ....
- Sensor:** (empty)
- Current range:** 100 pA, 1 nA, 10 nA, 100 nA, 1 uA, 10 uA, 100 uA, 1 mA, 10 mA
- Pretreatment settings:**
  - E condition: 0.0 V
  - t condition: 0 s
  - E deposition: 0.0 V
  - t deposition: 0 s
- Cyclic Voltammetry settings:**
  - t equilibration: 8 s
  - E begin: 0.0 V
  - E vertex1: 0.5 V
  - E vertex2: -0.5 V
  - E step: 0.1 V
  - Scan rate: 1.0 V/s
  - Number of scans: 5
- Reverse when I <:** 0.0 uA
- Reverse when I >:** 0.0 uA
- Measure OCP:** (unchecked)

Figure 61: New voltammetry programme settings

The scan rate was changed from 0.1 V/s to 1.0 V/s and the E step from 0.01 V to 0.1 V (see figure 61).

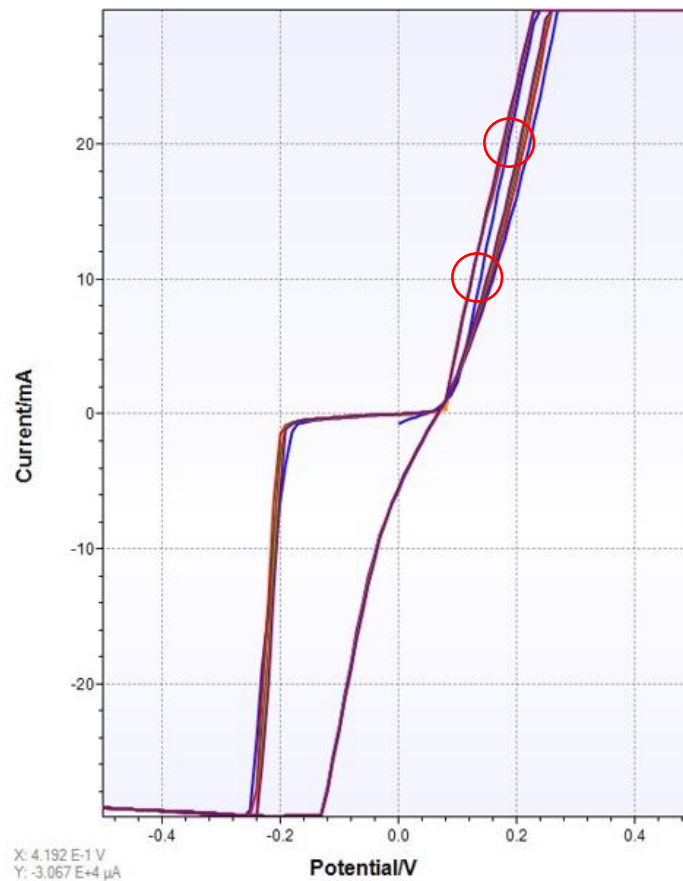


Figure 62: Voltammetry measurement of the own silver-silver chloride sphere with new settings

Two red points have been marked in figure 62. The points for determining the impedance were selected because the Howland source is limited to 10 mA. The second point was selected at the double overload limit, because it can also be shown here that the sphere can work well in this area. No selection can be made in the negative range because the hysteresis range is in effect. Zero mA cannot be selected either, because the hysteresis is already beginning. For the voltage and current difference and the  $\Delta I$  is 10 mA and the  $\Delta V$  is 0.06 V. This results in an impedance of  $6 \Omega$  according to equation (78). The hysteresis has become smaller by changing the programme settings. In the case of own chlorinated silver-silver chloride sphere, the layer is not optimal and this is the reason for the hysteresis. Next, a disposable electrode was tested. The result is better than with the own chlorinated silver-silver chloride sphere. According to the figure 63, the first loop (blue curve) of the measurement is different, because the electrode is forming up and then running in a steady state behaviour. The disposable electrode is linear.

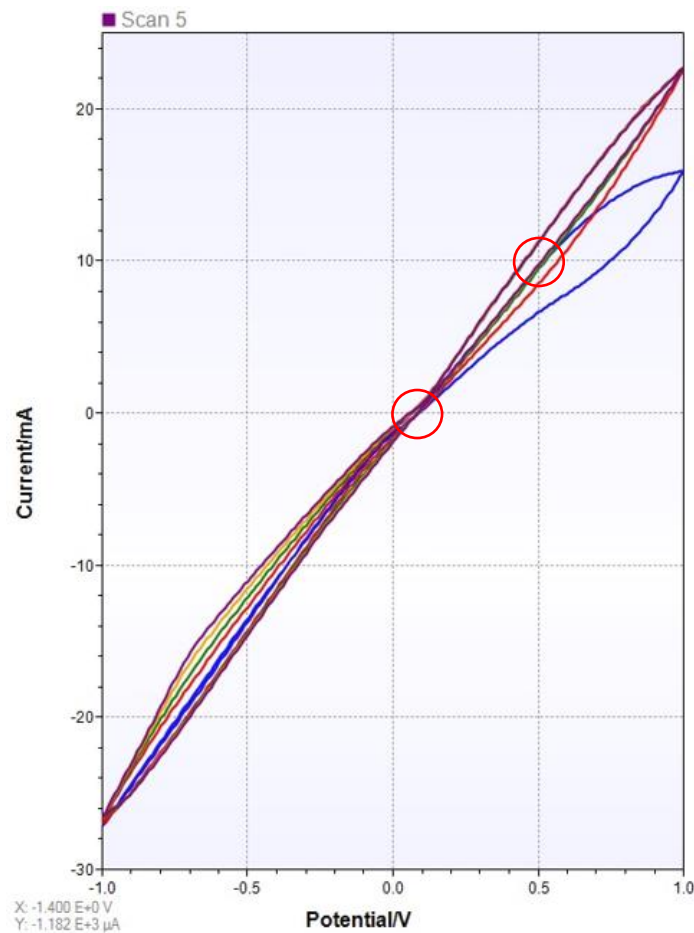


Figure 63: Voltammetry measurement of the disposable electrode silver-silver chloride electrodes

Two red points have been marked in figure 63. The points for determining the impedance were selected because the Howland source is limited to 10 mA. The second point was selected at 0 mA, because the hysteresis has not begun at 0 mA. For the voltage and current difference and the  $\Delta I$  is 10 mA and the  $\Delta V$  is 0.4 V. This results in an impedance of 40  $\Omega$  according to equation (78).

After a few measurements, one sphere in each of the three planes became lighter and the other three darker. This means that the silver chloride layer on the lighter side is degrading. The solution is to apply alternating current (reverse polarity). This can be controlled via the software. After the measurement has been completed, the signals fed in are rotated by 180° and fed back into the tank.

The disposable electrodes are connected to the cross using SMB sockets (see figure 64). The connecting wire was soldered to the socket and insulated with a 2-component adhesive (UHU PLUS ENDFEST 300).



Figure 64: Cross with disposable electrodes

### 3.4. Measurement of the entire system

As mentioned in section 2.2.1, a period is cut out of the data set and continuously replayed. For this reason, the end and the beginning of the signal do not match, resulting in a discontinuity. In reality this should not be the case. The problem was solved by using the `detrend` command in Matlab.



Figure 65: Einthoven leads of the patient patient245/s0480\_re [27]

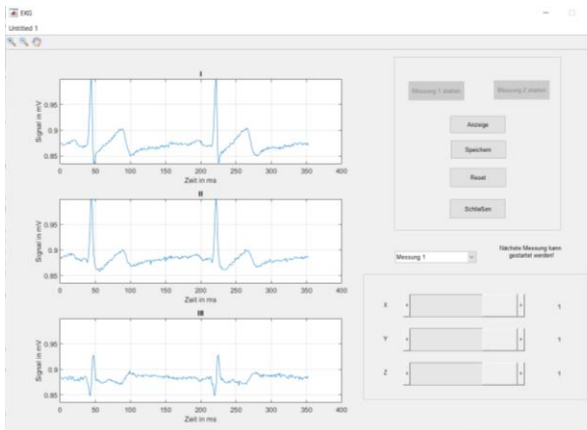


Figure 66: Measurement 1 with weighting  $x = 1$ ,  $y = 1$  and  $z = 1$



Figure 67: Measurement 2

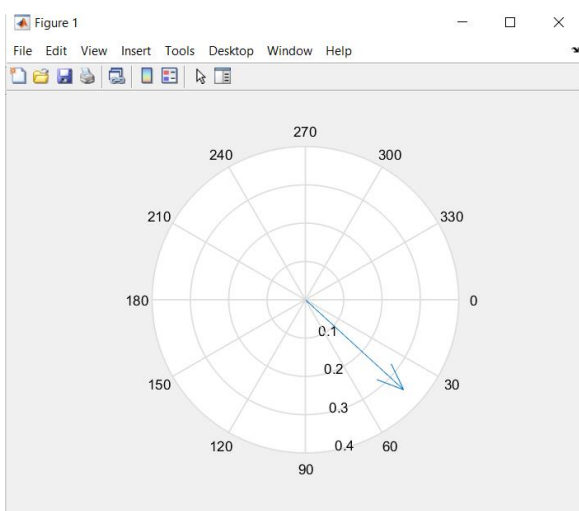


Figure 68: Axis type with weighting  $x = 1$ ,  $y = 1$  and  $z = 1$

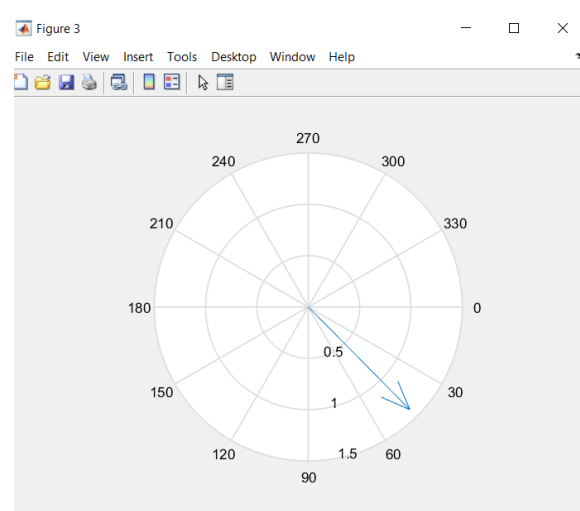


Figure 69: Axis type for measurement 2

In figure 66, measurement 1 was started with the weights  $x, y, z = 1$ . As can be seen in figure 66, the plots correspond well with figure 65. The axis type of the patient, with these settings, is an indifference type (see figure 68). The purpose of measurement 1 is to show that if a source signal is fed in different surface projections can be obtained by changing the weighting. This measurement is only used to show how the axis type can be changed by rotating the source vector, so it is not important which source signal is fed in. For this reason, the Frank derivative was fed in as the source vector and the Einthoven derivatives were measured. Measurement 1 is used to study how a different weighting of the components affects the position type.

Measurement 2, on the other hand, reconstructs the source vector from the measurement data of a real ECG signal. If this source vector is fed in, then this ECG signal should be measured again, under ideal assumptions. As mentioned in selection 2.1, the Einthoven leads of the measurement data are used for the reconstruction.

If the comparison of measurement 2 (see figure 67) with the original curve (see figure 65) show that leads I and II are almost identical. Lead III is significantly larger and the signal shape differs from the original time course of the patient (see figure 65). The axis type of measurement 2 is an indifference type (see figure 69).

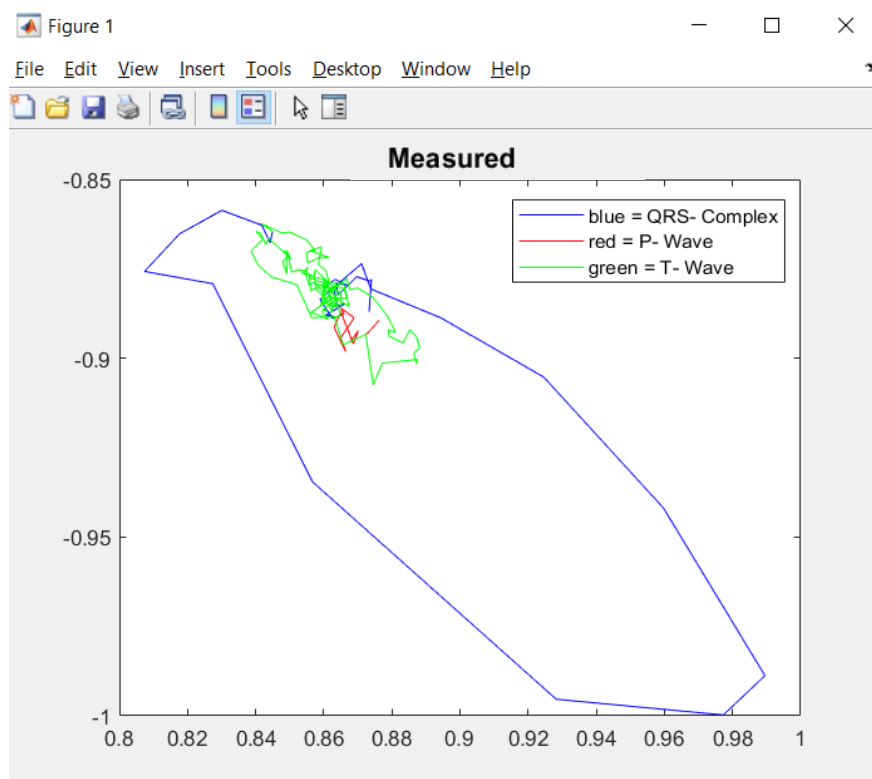


Figure 70: Measured vector loop measurement 2



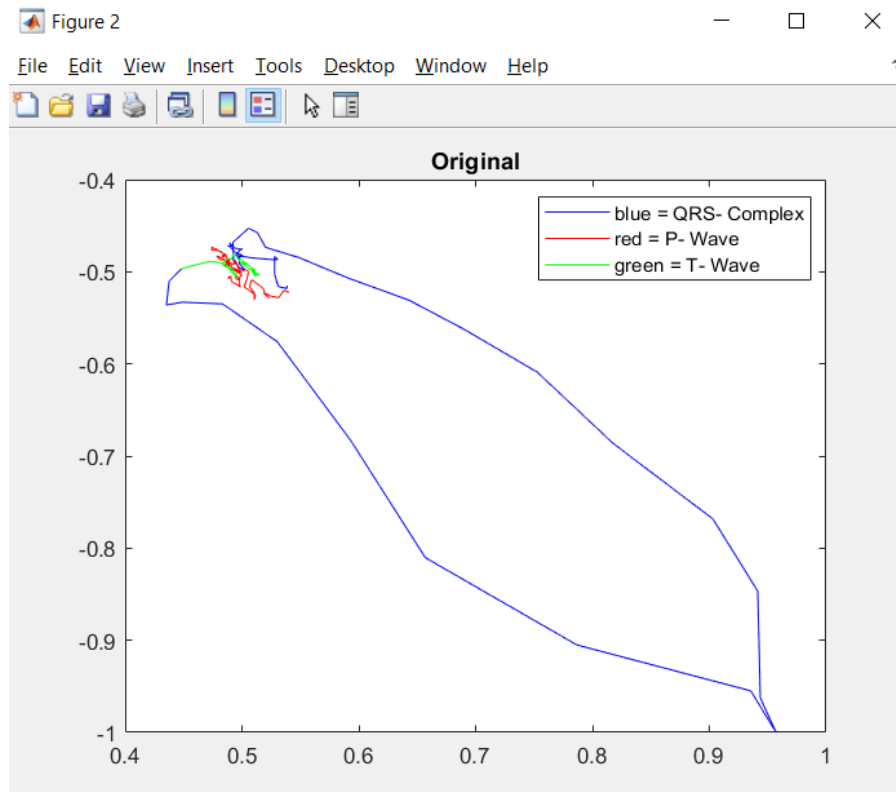


Figure 71: Original vector loop measurement 2

Figure 71 shows the original vector loop. The red segment is the P wave, the blue segment is the QRS complex and the green segment is the T wave. This applies to the measured vector loop in figure 70. A comparison of fig 70 and 71 yields a similar shape of the loops, though not identical. There is not only a difference in the shape, but also in the loop length. In the original vector loop, the P wave and the T wave are almost the same size and the QRS complex is narrower and has a spike. In the measured vector loop, the QRS complex is wider and does not have a pronounced spike, as in the original vector loop. Furthermore, the T wave is significantly larger than the P wave. This is due to the fact that the T wave is more pronounced than in the original recording of the patient.

## 4. Discussion

When injecting the source vector after reconstruction from a true ECG recording, the latter deviates from the measured one (see figure 65 and 67). The reason for this is that this is a finite thorax phantom and not an infinitely extended sphere as Einthoven assumed. Therefore, this cannot be the true heart vector and there must be a deviation. This is didactically valuable as it shows the influence of the used model on the results. The experiment could be repeated after changing the conductivity distribution inside the phantom, e.g. by inserting air-filled voids mimicking the lungs.

As in section 2.4, several Howland sources were tested and the only variant that fulfils the "Push & Pull" specification and the  $180^\circ$  phase shift of the sources and sinks was selected. With the Howland sources, it should be noted that precision resistors (at least 0.1% tolerance) are used and that a capacitor, a few pF to nF depending on the application, is connected in parallel in the feedback path. Also as described in selection 2.4, the resistance ratio in the feedback and feedback path must be the same, so that gain is only dependent on the shunt resistance. The capacitor of the lowpass filter of the offset compensation causes a produces a phase shift between the two signals. After removing the capacity the compensation works.

For the receiver unit, it is important that a high-pass filter is fitted to the inputs of the instrumentation amplifier. It is recommended that the complete filter stage is connected before the instrumentation amplifier, as possible noise and interference outside the ECG band are suppressed in advance. A further improvement could also be made, namely to use the active filter instead of the passive filter, as the instrumentation amplifier has almost reached its limits with its amplification. This would allow the received signal to be amplified more and thus displayed in greater detail. The Driven Right Leg (= DRL) and the notch filter were not tested, because the interferences are low. The reference potential of the tank is connected to the ground of the main board (virtually generated ground).

The custom- made electrodes though much better than those made from brass, gold or stainless steel, did not yet meet the expectations. The disposable electrodes are the best and simplest solution. Furthermore, a resistant 2-component adhesive should be sought. The salt solution causes the adhesive to slowly dissolve after around six weeks

and the insulation is therefore lost. Since the laboratory course is conducted over the entire summer semester, it would be possible to make several crosses and exchange them as needed or find a better insulating material.

The GUI interface could be improved by positioning the buttons and pop-up menu differently. Furthermore, only one measurement button could be set up, as there is a pop-up menu. Furthermore, a measurement button could be set up with just one button, since a pop-up menu is available. In the same way, an automatic reset for measurement 2 can also be installed, i.e. when the measurement button is pressed, a reset of the GUI can be carried out beforehand. An automatic reset for measurement 1 is difficult to implement, as the slide bars would also be reset automatically and therefore no weighting could be added to the signal. In addition, an STM32 with a larger memory could be used. This would mean that only every third value would have to be taken after the function calculations. Another idea for the future is to program the GUI in Python, for example.

An error that occurred on the main circuit board (Howland current sources and instrumentation amplifier) was that the photolithography mask for the bottom layer of the circuit board had been displaced slightly during manufacture. Another suboptimal design was, that the bottom layer is not connected to ground, but to the supply voltage of +11.3 V, which should be avoided. Furthermore, more test points or test pads should be added to make troubleshooting easier.

In conclusion, it can be said that the hardware and software set up works and the laboratory exercise, reconstruction of the vectorcardiogram and the standard leads according to Einthoven with axis type determination, is carried out.

## 5. Literature

- [1] “What is a MATLAB GUI?”, mathworks.com, available online at: <https://de.mathworks.com/discovery/matlab-gui.html> (last accessed on 26.06.2022)
- [2] “guide”, mathworks.com, available online at: [https://de.mathworks.com/help/matlab/ref/guide.html#:~:text=guide%20opens%20GUI%2C%20a%20UI,laying%20out%20and%20programming%20UIs.&text=guide\(%20filename%20\)%20opens%20the%20specified,file%20for%20editing%20in%20GUIDE.](https://de.mathworks.com/help/matlab/ref/guide.html#:~:text=guide%20opens%20GUI%2C%20a%20UI,laying%20out%20and%20programming%20UIs.&text=guide(%20filename%20)%20opens%20the%20specified,file%20for%20editing%20in%20GUIDE.) (last accessed on 26.06.2022)
- [3] V. G. Sirtoli, K. F. Morcelles, V. C. Vincence: Design of current sources for load common mode optimization. Journal of Electrical Bioimpedance Vol. 9: 59 – 71 (2018), available online at: <https://www.sciendo.com/article/10.2478/joeb-2018-0011> (last accessed on 02.07.2022)
- [4] “Ableitungssysteme von EKGs”, cardiosecur.com, available online at: <https://www.cardiosecur.com/de/ihr-herz/fachartikel-rund-um-das-herz/ableitungssysteme-von-ekgs> (last accessed on 03.07.2022)
- [5] F. Maxner (2017), *Implementierung eines Interface zur Generierung von realistischen EKG Signalen in einem Thoraxphantom* (Bachelorarbeit, TU Graz Biomedical Engineering)
- [6] “STM32G474RE Mainstream Arm Cortex-M4 MCU 170 MHz with 512 Kbytes of Flash memory, Math Accelerator, HR Timer, High Analog level integration”, st.com, available online at: <https://www.st.com/en/microcontrollers-microprocessors/stm32g474re.html> (last accessed on 23.06.2022)
- [7] STMicroelectronics (2018), STM32F334x4 STM32F334x6 STM32F334x8 Datasheet, available online at: <https://www.st.com/resource/en/datasheet/stm32f334c8.pdf> (last accessed on 23.06.2022)
- [8] STMicroelectronics (2020), UM1724 User manual STM32 Nucleo-64 boards (MB1136), available online at: [https://www.st.com/resource/en/user\\_manual/um1724-stm32-nucleo64-boards-mb1136-stmicroelectronics.pdf](https://www.st.com/resource/en/user_manual/um1724-stm32-nucleo64-boards-mb1136-stmicroelectronics.pdf) (last accessed on 18.12.2022)

- [9] Texas Instruments (2013), AN-1515 A Comprehensive Study of the Howland Current Pump Application Report, available online at: <https://www.ti.com/lit/an/snoa474a/snoa474a.pdf> (last accessed on 28.06.2022)
- [10] Jinzhen Liu, Xiaoyan Qiao, Mengjun Wang, Weibo Zhang, Gang Li, and Ling Lin: *The differential Howland current source with high signal to noise ratio for bioimpedance measurement system*. Review of Scientific Instruments 85, 055111 (2014), available online at: [https://aip.scitation.org/doi/pdf/10.1063/1.4878255?casa\\_token=Ym9zkarcy8IAAAAA:AXyDFLuuYiqjIV2UC1qJkDKT81M6e3oXjeZJZKfbn\\_fKlwrDPS-LVcMBLRQIFT2Z3ksrSrek36gL4g](https://aip.scitation.org/doi/pdf/10.1063/1.4878255?casa_token=Ym9zkarcy8IAAAAA:AXyDFLuuYiqjIV2UC1qJkDKT81M6e3oXjeZJZKfbn_fKlwrDPS-LVcMBLRQIFT2Z3ksrSrek36gL4g) (last accessed on 02.07.2022)
- [11] B.Eng. Ph. Gräbner (2016), Entwicklung einer steuerbaren Stromquelle mit Parameterüberwachung (Abschlussarbeit zur Erlangung des akademischen Grades Master of Engineering (M.Eng.), Forschungs- und Transferzentrum Leipzig e.V.)
- [12] Texas Instruments (2022), LMx58-N Low-Power, Dual-Operational Amplifiers Datasheet, available online at: [https://www.ti.com/lit/ds/symlink/lm358-n.pdf?ts=1725880988373&ref\\_url=https%253A%252F%252Fwww.ti.com%252Fproduct%252FLM358-N](https://www.ti.com/lit/ds/symlink/lm358-n.pdf?ts=1725880988373&ref_url=https%253A%252F%252Fwww.ti.com%252Fproduct%252FLM358-N) (last accessed on 06.03.2022)
- [13] H. Zumbahlen et al., "Db Compression Point", sciencedirect.com, available online at: <https://www.sciencedirect.com/topics/engineering/db-compression-point> (last accessed on 13.09.2024)
- [14] Datei:Elektrochemische Dreielektrodenmessenordnung.svg, de.wikipedia.org, available online at: [https://de.wikipedia.org/wiki/Datei:Elektrochemische\\_Dreielektrodenmessenordnung.svg](https://de.wikipedia.org/wiki/Datei:Elektrochemische_Dreielektrodenmessenordnung.svg) (last accessed on 10.12.2024)
- [15] Burr- Brown (1993), INA115 Precision INSTRUMENTATION AMPLIFIER Datasheet, available online at: <https://www.ti.com/lit/ds/symlink/ina115.pdf?ts=1726664255845> (last accessed on 06.04.2021)
- [16] Texas Instruments (2024), INA114 Precision Instrumentation Amplifier Datasheet, available online at:

[https://www.ti.com/lit/ds/symlink/ina114.pdf?ts=1726648115444&ref\\_url=https%253A%252F%252Fwww.mouser.it%252F](https://www.ti.com/lit/ds/symlink/ina114.pdf?ts=1726648115444&ref_url=https%253A%252F%252Fwww.mouser.it%252F) (last accessed on 03.04.2021)

[17] “Bandsperrfilter”, electronics-tutorials.ws, available online at: <https://www.electronics-tutorials.ws/de/filtren/bandsperrfilter.html> (last accessed on 05.05.2021)

[18] R. Elliott, “Simple DC Adapter Power Supply”, sound-au.com, available online at: <https://sound-au.com/project43.htm> (last accessed on 24.09.2023)

[19] “Using 12V DC to create symmetric power source”, electronics.stackexchange.com, available online at: <https://electronics.stackexchange.com/questions/219827/using-12v-dc-to-create-symmetric-power-source> (last accessed on 24.09.2023)

[20] Ch. Knoblauch, „Impedanzspektroskopie – Ein Überblick von der Theorie bis zur Anwendung“, wotech-technical-media.de, available online at: [https://www.wotech-technical-media.de/womag/ausgabe/2015/09/31\\_knoblauch\\_impedanz\\_09j2015/31\\_knoblauch\\_impedanz\\_09j2015.php](https://www.wotech-technical-media.de/womag/ausgabe/2015/09/31_knoblauch_impedanz_09j2015/31_knoblauch_impedanz_09j2015.php) (last accessed on 23.10.2022)

[21] L. J. Längle (2019), *Numerische Simulation eines homogenen Thoraxmodells zur Demonstration der elektrischen Feldverteilung bei EKG Ableitungen* (Bachelorarbeit, TU Graz Biomedical Engineering)

[22] P. Kurzweil, *Angewandte Elektrochemie*, 1. Auflage Springer Fachmedien Wiesbaden GmbH, 2020, available online at: <https://link.springer.com/content/pdf/10.1007/978-3-658-32421-6.pdf> (last accessed on 25.01.2023)

[23] “Electrodes used with a potentiostat”, palmsens.com, available online at: <https://www.palmsens.com/knowledgebase-article/electrodes-of-a-potentiostat/?compare=2106> (last accessed on 28.01.2023)

[24] “Cyclic Voltammetry 2/4- What is a Cyclic Voltammogram?”, palmsens.com, available online at: <https://www.palmsens.com/knowledgebase-article/cyclic-voltammetry-what-is-a-cyclic-voltammogram/?compare=2106> (last accessed on 14.09.2024)

- [25] "Silberchlorid", chemie.de, available online at: <https://www.chemie.de/lexikon/Silberchlorid.html#Nachweis> (last accessed on 08.09.2024)
- [26] "STM32F334C8 Mainstream Mixed signals MCUs Arm Cortex-M4 core with DSP and FPU, 64 Kbytes of Flash memory, 72 MHz CPU, CCM, 12-bit ADC 5 MSPS, comparators, op-amp, hr timer", st.com, available online at: <https://www.st.com/en/microcontrollers-microprocessors/stm32f334c8.html> (last accessed on 23.06.2022)
- [27] "PHYSIOBANK ATM", archive.physionet.org, available online at: <https://archive.physionet.org/cgi-bin/atm/ATM> (last accessed on 01.09.2024)
- [28] "USART", user.tu-chemnitz.de, available online at: <https://www-user.tu-chemnitz.de/~heha/hsn/chm/ATmegaX8.chm/20.htm> (last accessed on 19.09.2024)
- [29] "Natrium", spektrum.de, available online at: <https://www.spektrum.de/lexikon/chemie/natrium/6137#:~:text=Natrium%2C%20Symbol%20Na%2C%20chem.,g%20cm%2D3%2C%20F> (last accessed on 15.09.2024)
- [30] "Chlor", spektrum.de, available online at: <https://www.spektrum.de/lexikon/chemie/chlor/1761> (last accessed on 15.09.2024)
- [31] "Molare Leitfähigkeit", interaktiv.chemie.uni-mainz.de, available online at: <https://interaktiv.chemie.uni-mainz.de/vpcgp/ml-man.de.html> (last accessed on 15.09.2024)
- [32] Dr. Ch. Eisenhut, "Die Größe "Stoffmengenkonzentration", lernort-mint.de, available online at: <https://www.lernort-mint.de/chemie/angewandte-chemie/stoffmengenkonzentration/> (last accessed on 15.09.2024)
- [33] "Electrodes used with a potentiostat", palmsens.com, available online at: <https://www.palmsens.com/knowledgebase-article/electrodes-of-a-potentiostat/?compare=2106> (last accessed on 06.12.2024)